RESEARCH

Benchmarking study of 10 MW TLB floating offshore wind turbine

Iman Ramzanpoor[1] · Martin Nuernberg[2] · Longbin Tao[1]

© Crown 2023

Abstract

This paper presents a benchmarking study of four floating wind platform' motion and dynamic tension responses to verify an innovative design with the intention of overall cost reduction of a durable, reliable, safe design. An aero-hydro-servo-elastic code is applied to benchmark a 10 MW tension leg buoy (TLB) floating wind turbine to the current leading technology types for floating offshore wind platforms, specifically spar buoy, Semi-submersible and tension leg platform (TLP) floating wind turbines. This study assumes that the platforms will deploy in the northern region of the North Sea, with a water depth of 110 m under various environmental conditions, including wind field descriptions covering uniform wind to fluctuating turbulent wind. The obtained dynamic response results showed low motion responses for the TLB platform for all design load cases. More specifically, the TLB surge and pitch motion responses are insignificant under both operational and survival conditions, allowing decreased spacing between individual wind turbines and increasing wind farms' total energy generation capacity. An additional benefit is that the wind turbine systems can be installed without significant pitch modification to the control system. The TLB platform is less complex which simplifies the construction process and has the potential for significant cost reductions.

Keywords Floating wind turbines · Tension leg buoy (TLB) · Spar · Semi-submerisble · TLP · Aerodynamics and hydrodynamics · Taut and catanery mooring

Abbreviations

FOWT	Floating offshore wind turbine
TLB	Tension leg buoy
TLP	Tension leg platform
COG	Centre of gravity
COB	Centre of buoyancy
LCOE	Levelized cost of energy
SWL	Still water level
NTM	Normal turbulence wind
EWM	Extreme wind model
DLC	Design load case
NSS	Normal sea state
SSS	Severe sea state
ESS	Extreme sea state

✉ Longbin Tao
longbin.tao@strath.ac.uk

1 Department of Naval Architecture, Ocean and Marine Engineering, University of Strathclyde, Glasgow G4 0LZ, UK

2 Newcastle Marine Services Ltd., Newcastle Upon Tyne NE12 9SZ, UK

1 Introduction

The use of floating foundations to support a wind turbine represents an innovative solution to existing depth restraints in the industry. Currently, most offshore wind turbines are fixed to the seabed by monopile or jacket foundations and, as a result, are restricted to a range of water depths of up to 40–60 m (Henderson et al. 2002; Carbon Trust 2015; CATAPULT 2018). It is estimated that approximately 80% of offshore wind resources are located in water depths of 60 m and beyond (Myhr et al. 2014; Zhao et al. 2012), where traditional bottom fixed offshore wind turbine is not economically appealing (Henderson and Witcher 2010). In this context, the offshore wind energy community must confront the challenge of developing cost-efficient support structures for a broader scope of installation sites (Leimeister et al. 2018). The design of such cost-efficient support structures strongly depends on a proper prediction of extreme loads, which are only possible with aero-hydro-elastic simulation codes that can account for the entire system's dynamic behaviour under simultaneous aerodynamic hydrodynamic loading (CATAPULT 2018; Matha et al. 2015). The elimination of depth

constraints and improved turbine setup could open other power generation paths in deeper waters further offshore (Zwick and Muskulus 2016).

Floating platforms for wind turbines have been proposed for many years (Witte et al. 2003), but only recently has the technology matured sufficiently to consider overcoming the technical challenges required to design a commercial system (Maciel 2010; Statoil 2017; Fukushima Offshore 2014). The long-term survivability of floating structures has been successfully demonstrated over decades; however, the economics that allowed the mass-production deployment of offshore oil and gas rigs has yet to be demonstrated for floating wind turbine platforms (CATAPULT 2015). The offshore oil and gas industry has proven that technical challenges can be overcome. However, the economics of implementing the oil and gas industry's solution would not be cost-effective for the deployment of a floating wind turbine in a competitive wind energy market (Butterfield et al. 2007). Platform designs for offshore wind require adaptation to accommodate different dynamic characteristics and a distinct loading pattern. The three main concepts for floating foundations (Spar-Buoy, Semi-submersible and TLP)) have varying dynamic characteristics, each with its pros and cons concerning performance, cost and system complexity (International renewable Energy Agency (IRENA) 2016; Castro-Santos and Diaz-Casas 2016; Butterfield et al. 2007; Borg and Collu 2015; Taboada 2015).

A Spar platform is a cylinder with a low waterplane area that uses ballast to keep the centre of gravity below the centre of buoyancy. It is kept in position primarily by catenary mooring lines with drag or suction anchors. It has a tendency for lower critical wave-induced motions, a simple design and low installed mooring cost. On the other hand, offshore operations require heavy-lift vessels and currently can be undertaken only in relatively sheltered, deep water. The Spar platform needs deeper water than the other design types, typically greater than 100 m (Bossler 2013; Nilsson and Westin 2014; James and Rose 2015; Mast et al. 2015). The first Spar wind turbine was demonstrated in Norway in 2009 (2.3 MW Hywind), and a number 5 MW version was installed in the Hywind demonstrator farm in Scotland in 2017. A floating wind farm with a 30 MW power generation capacity at more than 100 m water depth has been operated (Equinor 2018). Following the Statoil (Hywind) demonstration in Norway in 2013, Japan Marine United demonstrated an advanced (hybrid) 2 MW Spar, supporting floating substations, in partnership with Kyoto University, Sasebo Heavy Industries, and Nippon Hume, amongst others. This was followed by the installation of a 5 MW capacity Spar in 2016. Other previous examples of this type of Spar include (Paulsen et al. 2012), SeaTwirl (Singhal et al. 2021) and Windcrete (Mahfouz et al. 2021).

Semi-submersible support platforms are made from several large columns, each linked by connecting bracings and submerged pontoons. Columns provide hydrostatic stability, whilst the pontoons provide additional buoyancy. The platform is usually positioned by catenary or taut spread mooring lines and drag anchors. Fully outfitted platforms, including turbines, can be floated with drafts below 10 m to aid transportation using conventional tugs. It can be used in water depths of approximately 40 m but tends to be subjected to higher critical wave-induced motions. These platforms are generally larger structures with higher fabrication complexity than other concepts, especially Spar buoys (Mast et al. 2015; Kolios et al. 2016; James et al. 2018). Examples of this type include; the Principle Power (WindFloat), demonstrated in Portugal in 2011 (2 MW) (Cermelli et al. 2012), and Fukushima FORWARD, demonstrated in Japan in 2013 (2 MW) and 2015 (7 MW) (Rodrigues et al. 2015). In addition, the 50 MW Kincardine offshore wind farm is located Scotland operated since October 2021 (Principle-Power 2022). The use of this design type continued with Ideol (Floatgen) 2 MW (Alexandre et al. 2018), Hexicon 5 MW (Amano 2017), Pentland Floating Offshore Wind Farm (PFOWF) (PFOWF 2022).

A TLP is a highly buoyant floating platform with a central column and arms connected to tensioned tendons (Liu et al. 2016). These tendons are usually connected to suction pile anchors, which secure the platform. TLPs generally have a low mass, with a tendency for lower critical wave-induced motions. It can be used in water depths of 50–60 m, depending on metocean conditions (Henderson and Witcher 2010; Mast et al. 2015). Compared to other platforms, it is harder to keep stable during transport and installation depending on the design, and a special-purpose vessel may be required. There remain uncertainties about the impact of possible high-frequency dynamic effects on the turbine when using this support platform design. In addition, the installed mooring cost is higher compared to catenary mooring line installation due to the complexity of pre-tensioning the tendons (Musial et al. 2006; Butterfield et al. 2007). GICON is the first TLP floating wind technology commercial operator, demonstrated in Germany in 2016, with a capacity of 2.3 MW (Adam et al. 2014). Another example is the PelaStar (capacity 6 MW), developed by Glosten Associates (Vita et al. 2015); the project involves designing and developing advanced controls for a 12 MW floating wind turbine in 2019.

Whilst these three concepts are widespread in academic and industrial research, the optimum platform does not yet exist. The challenges faced by platform designers include design tool limitations and methodology, cost/complexity of the support structure, design of the buoyancy tanks and design of the mooring system. Other important challenges concerning FOWT design is accurately predicting their time-dependent power output, dynamic system responses and

structural loadings under variable wind and wave conditions (Liu et al. 2017).

The analysis of coupled dynamics of floating support structures is complex. Jonkman (Jonkman and Sclavounos 2006) and Hansen (Jonkman and Buhl 2007a, b) proved that the analysis could be done by combining wind turbine aeroelastic codes with a hydrodynamic module. Recently, various studies have used linear frequency-domain analysis, commonly employed in the offshore oil and gas industry (Bulder et al. 2002; Lee 2005; Wayman et al. 2006; Roald et al. 2013). However, these studies have one obvious limitation: the nonlinear dynamic characteristics and transient events that are essential considerations in the analysis of wind turbines cannot be captured. Several offshore floating wind turbine studies have attempted to address this knowledge gap (Jonkman and Buhl 2007a, b). For example, Fulton et al. (2006) and Withee (2004) used different time-domain aeroelastic wind turbine simulators to include the effects of platform motion and hydrodynamic loading of Semi-submersible and TLP designs for a 5 MW turbine, respectively. This showed that platform motions have little effect on power capture and rotor loads. Instead, these characteristics are dominated by the aerodynamics of the rotor. The limitations of previous time and frequency domain studies on floating offshore wind turbines motivated the development of simulation capability for modelling such systems in fully coupled aero-hydro-servo-elastic response. This study aims to introduce an investigation and verification of aero-hydro-elastic codes for benchmarking 10 MW TLB offshore floating wind turbines by comparing the use of three common floating offshore wind turbine (FOWT) types. Furthermore, this study presents the dynamic responses and mooring line loadings resulting from the aero-hydro-elastic code simulation, where each design is exposed to variable wind and wave conditions.

The paper is organised as follows: Sect. 2 describes the floating systems, followed by Sect. 3 introducing the methodology and numerical methods that are used for fully coupled aero-hydro-elastic analysis. Section 4 describes the environmental loading conditions, followed by detailed results and discussions of the findings in Sect. 5. The projects conclusions are presented in Sect. 6.

2 Floating systems

Four types of floating systems (Spar, Semi-submersible, TLP, and TLB) are considered in this study, with each design scaled to support a 10 MW wind turbine using an appropriate methodology (George 2014) to be able to have the same energy generation. Each system is then attached to the seabed by mooring lines to keep position, again using an appropriate methodology (Al-Solihat et al. 2016). Figure 1 illustrates the
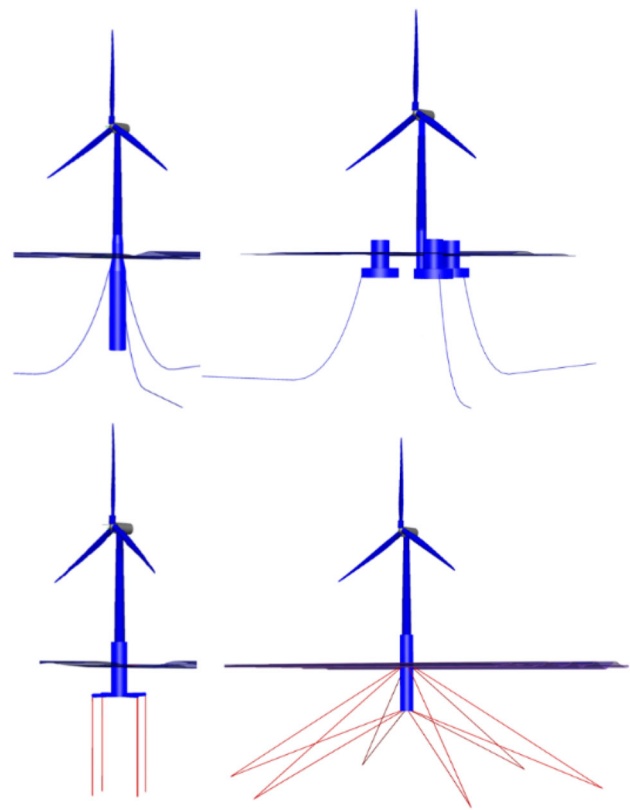

Fig. 1 Offshore floating concepts, clockwise from top-left: Spar, Semi-Submersible, TLB, and TLP

four systems.

2.1 Wind turbine

The DTU 10 MW is frequently used as a reference design in numerous research studies on offshore wind turbine simulation and numerical tools benchmarks. The DTU 10 MW was designed within the framework of the Light Rotor project in 2012 (Bak et al. 2013). However, this development only covers the details of an onshore-based turbine. Therefore, the characteristics of the tower must be adjusted for floating offshore platform applications, primarily by shortening the total tower length, measured as the distance between the top of the floater and the underside of the nacelle. This study shortened the total tower length to fit between the top of the floater at 20 m above sea level and the underside of the nacelle at 116 m above sea level. Shortening the total tower length can be achieved either by altering the ratio of the tower masses or by modifying the height ratio (George 2014).

2.2 Floating platforms

The process of scaling up the Semi-submersible and Spar systems is based on George's (2014) methodology. This uses a mass-depending factor, resulting in the "scaled design" followed by a modification to ensure the draft remains the same as the original non-scaled design; this is after that referred to as the "reduced draft design". The main difference between the scaled and the reduced draft design lies in the geometry of the offset columns for a Semi-submersible system. The offset columns' relative position to each other and the central column of the platform stays unchanged for the respective power rating of the system. The reduced draft design for both is lighter and will reduce material costs. The overall weight of the systems is kept constant by adjusting the amount of ballast water.

The Semi-submersible system was developed based on the 5 MW platform used in the OC4- OC4-DeepCwind project phase II (Offshore Code Comparison Collaboration Continuation) (Robertson et al. 2014). The Spar system was based on the OC3-Hywind Spar-Buoy, which used the turbine specifications of the National Renewable Energy Laboratory (NREL) offshore 5 MW baseline wind turbine (Jonkman et al. 2010).

The TLP system is scaled up to support the 10 MW DTU wind turbine based on a 5 MW TLP designed and developed from the Massachusetts Institute of Technology (MIT) design (Tracy 2007), referred to as MIT/NREL TLP herein (Coulling et al. 2013). Using methodology introduced as the Aina Crozier TLP transported methodology (Crozier et al. 2011).

TLB systems are designed to rely on excess buoyancy and mooring stiffness for their stability. Therefore, the most critical consideration when scaling this type of platform from previous studies (Sclavounos et al. 2010) is ensuring its excess buoyancy levels remain sufficient. The TLB platform modelled in this paper is developed from the concept proposed by Sclavounos et al. (2010), and later by Myhr et al. (2011) and Myhr (2016). The platforms' excess buoyancy and mooring stiffness are gradually increased by varying the dimensions of the platform and the mooring line's radii to ensure satisfactory performance concerning motion and mooring characteristics in both operational and survival conditions (Ramzanpoor et al. 2019). For the initial TLB model, the ratio between excess buoyancy and weight is constant between the 5 MW and 10 MW models. Later simulations and design iteration are completed with various design modifications. These modifications to the preliminary design led to improved performance of the platform in operating conditions and its survival, given extreme events (Ramzanpoor 2023).

The platforms characteristics of the four different designs are presented in Table 1. The mass value illustrates in Table 1

Table 1 10 MW offshore wind turbine support platforms description

Platform	Draft (m)	Mass (T)	COG (m)
Semi-Submersible	20	2645.3	13.5
Spar	85	13,450.7	− 51.4
TLP	27	2068.8	22.6
TLB	52	791	50.8

includes the ballasting weight. Also shown is the calculated centre of gravity for each, calculated for the complete system, including the tower, rotor and nacelle, and mooring weights.

The schematic drawing of four systems is shown in Fig. 2. One of the first proposed designs for large offshore structures was the TLB concept, which met the challenges highlighted whilst delivering the advantages of mass production (Sclavounos et al. 2010). In the floating offshore wind industry, the overriding focus is on driving costs down, and mass production allows the reduction of the Levelized Cost of Energy (LCOE). Therefore, simplicity and probabilistic design become essential. The TLB has significantly lower steel mass in the floater than other platform types applied to water depths deeper than 50 m, and the cost is potentially lower. However, the anchors are subject to relatively high mean horizontal and vertical loads due to taut mooring lines and excessive buoyancy. Furthermore, load variations due to wind and waves are transferred directly to the anchors, leading to higher anchor costs than conceptual designs with a catenary mooring line system. Additionally, TLB platforms do not require any ballasting in their operational condition. In comparison, Spar systems require solid and water ballasting (typically using iron ore and water), Semi-submersible systems use water ballast, and the TLP system uses concrete ballast. The ballasting of each system, where required, is shown in Fig. 2.

2.3 Mooring system

The Spar and Semi-submersible platforms' catenary mooring systems are similar to the Hywind 6 MW. The platforms are moored to the seabed using a conventional 3-line mooring. The mooring system for a TLP system consists of four tethers, and the mooring system applied to the TLB is a taut-leg mooring system similar to that presented in Trolle and Hornbak (2016). Mooring system configurations of the platforms are shown in Fig. 3 (where *L* is an abbreviation form to represent Line). Apart from the TLP mooring system, the mooring lines attach to the platform via a so-called "crowfoot" (delta connection) to increase the moorings' yaw stiffness (Robertson and Jonkman 2011). To simplify the analysis of the mooring system, several assumptions are made. Firstly, each multi-segmented line is replaced with an equivalent homogenous

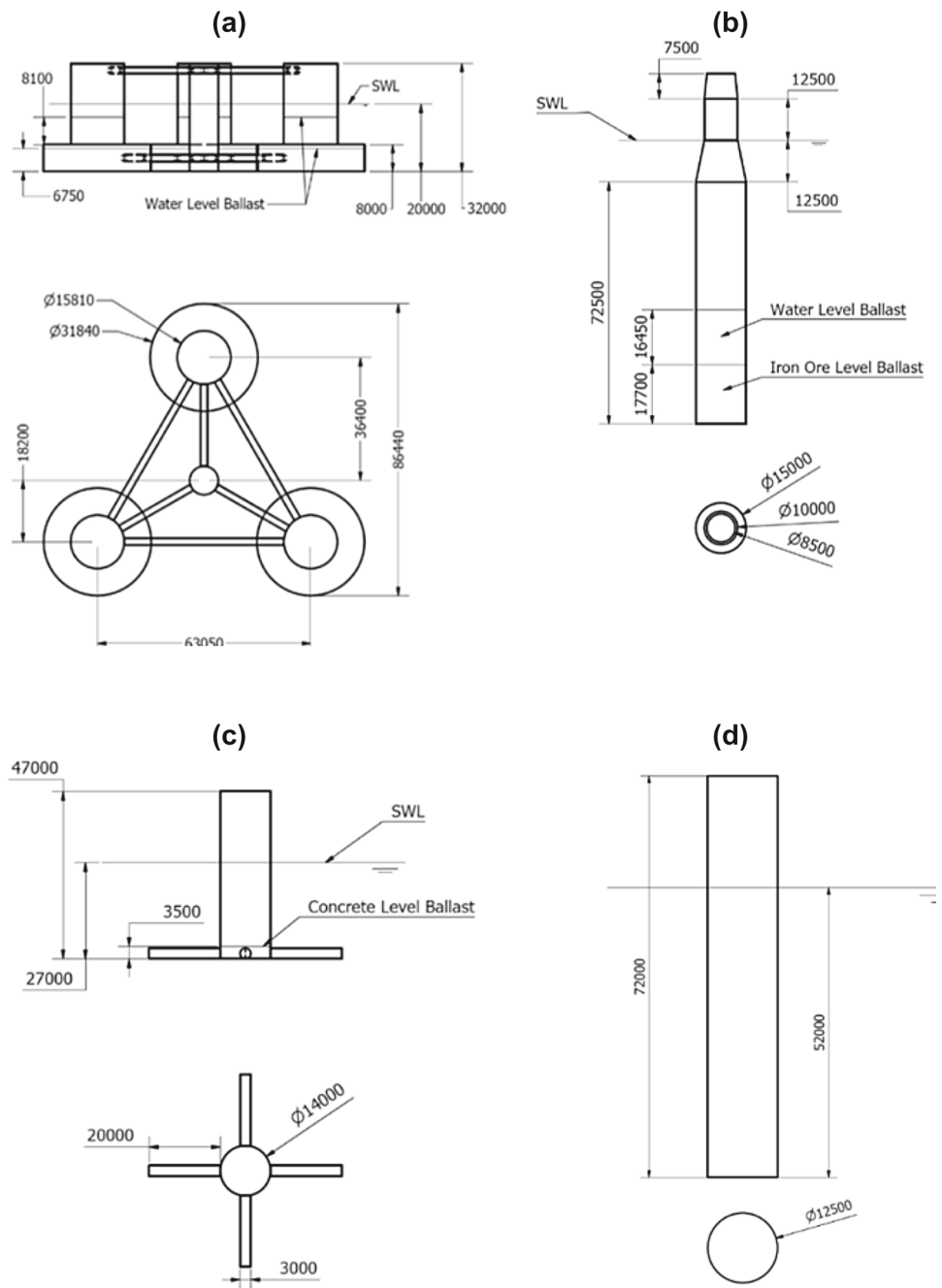**Fig. 2** Schematic top and side view of Semi-submersible (**a**), Spar (**b**), TLP (**c**), and TLB (**d**) platforms—all dimensions are in mm

Table 2 Mooring systems characteristics

Platform	Mooring type	Dimension (m)	Length (m)		Weight (kg/m)	MBL (N)
Semi-Submersible	Chain	0.166	857.6		400	2.73E+07
Spar			904.7			
TLP	Wire rope	0.48	83		494.5	6.38E+07
			Upper	Lower		
TLB		0.24	200.5	183.2	222	2.94E+07
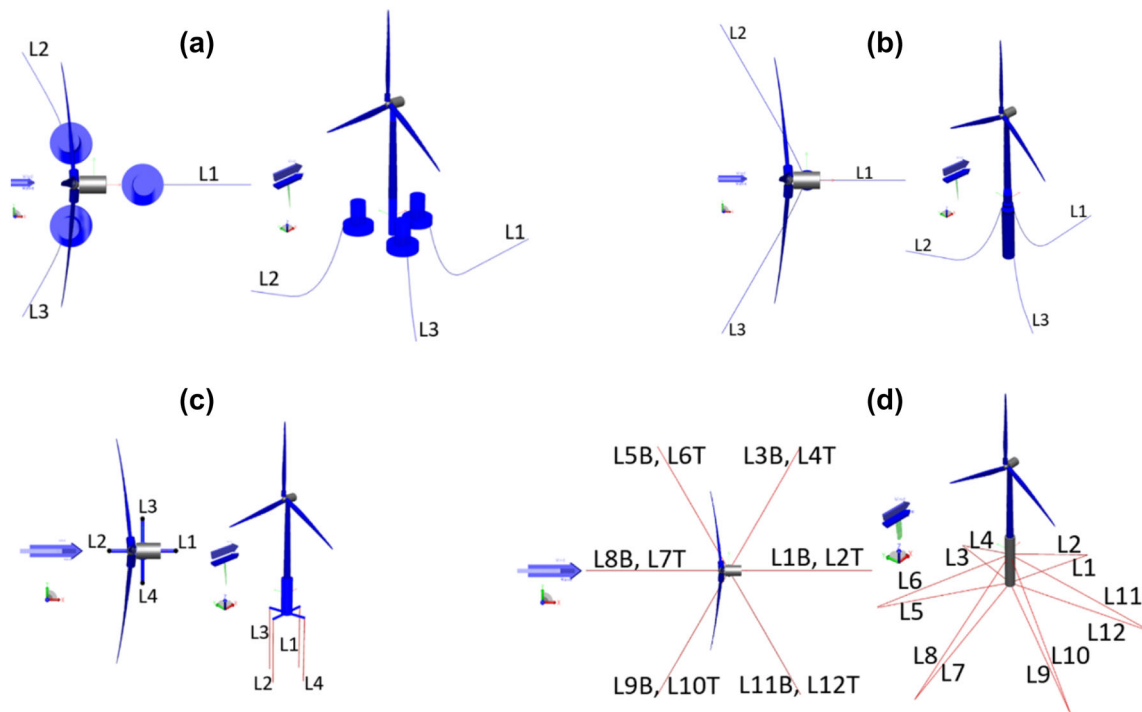
Fig. 3 Mooring system layout for Semi-submersible (**a**), Spar (**b**), TLP (**c**), and TLB (**d**) platforms—L, B, and T are the abbreviation formed of line, bottom and top

line, with properties derived as the weighted-average values of the mass, weight, and stiffness (weighted based on the unstretched lengths of each segment). Secondly, all mooring system damping, including the hydrodynamic and line-to-seabed drag, is neglected. For simplicity, a single attachment point for each mooring line was assumed and then modified according to the mooring system stiffness matrix, with an assumed angle of 20° spread of the attachment points to replicate the effects of a crowfoot connection to reduce the yaw motion of the platform (Al-Solihat et al. 2016).

The Spar system fairleads are located 12.5 m below the still water level (SWL) with a radius of 7.5 m from the platform centreline. The anchors are located 110 m below the SWL, at a radius of 853 m from the platform centreline. One line is directed along the positive x-axis (in the XZ-plane), with the two remaining lines distributed uniformly around the platform, such that each line, the fairleads, and the anchors are 120° apart when viewed from above (see Fig. 3b). Each of the three studless chain lines has an unstretched length of 902 m, a diameter of 0.166 m, an equivalent mass per unit length of 400 kg/m, an equivalent axial stiffness of 3.84243E+08 N, bending stiffness of 8.02E+07 Nm, and torsional stiffness of 6.3E+07 Nm/rad.

The Semi-submersible mooring system is similar to the Spar mooring system, but fairleads are located at a depth of 16 m below the SWL and a radius of 52.32 m from the platform centreline (see Fig. 3a). The anchor's radius is 806.2 m

from the platform centreline, with an unstretched length of 857.6 m and the same line properties as the Spar mooring line. The stiffness matrix for Spar and Semi-submersible is evaluated by the procedure presented in (Al-Solihat and Nahon 2016).

The mooring system designed for the TLP system uses four tethers anchored on the seabed (see Fig. 3c). In the horizontal plane of motion, the TLP behaves similarly to a floating structure, while in the vertical plane of motion, it is stiff and resembles a constrained fixed structure. A valid assumption is that the draft does not change, so the tether tension can be considered constant. In the taut leg mooring system, where the line does not contact the seabed but is taut due to the pretension caused by the excess buoyancy of the platform, most of the restoring loads are generated by line elasticity. The restoring coefficients are calculated by applying a small angle approximation whilst neglecting the tether mass. The procedure is presented in Crozier (2011). The tether is constructed of an 83 m-long steel wire rope with a diameter of 0.48 m. It has an equivalent mass per unit length of 494.5 kg/m with axial stiffness of 1.73E+10N. The TLP system fairleads are located 27 m below the SWL along a radius 27 m from the platform centreline, with the TLP stiffness matrix evaluated by the procedure presented in Al-Solihat and Nahon (2016).

The TLB mooring system is modified from Trolle and Hornbak (2016) by including a considerably larger anchor
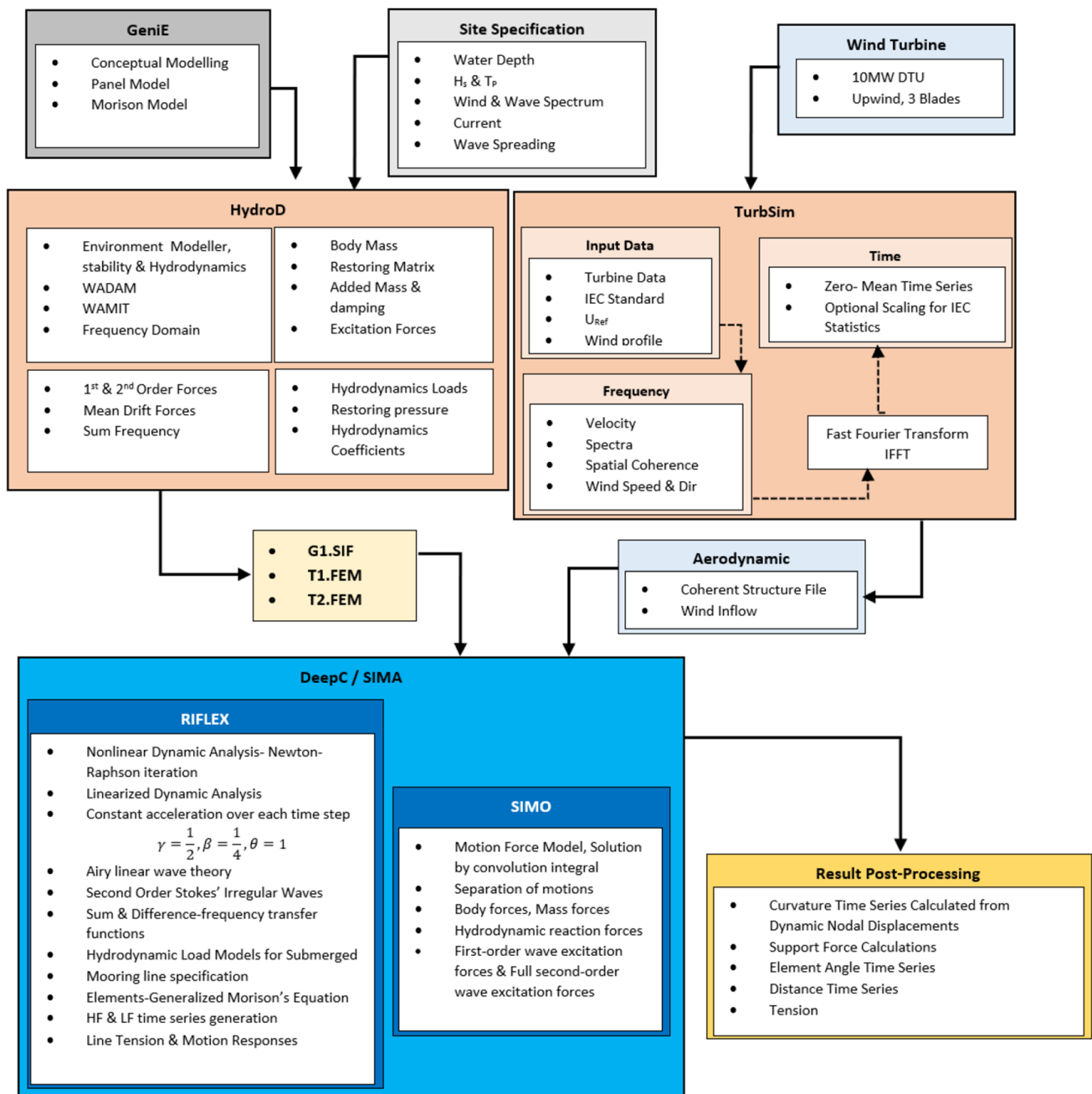
Fig. 4 Methodology flowchart

radius to allow anchor sharing in a farm of multiple floating wind turbines. The stiffness matrix of a mooring system composed of multiple lines is evaluated by summing the stiffness matrices of the individual lines following the procedure presented in Al-Solihat study (Al-Solihat and Nahon 2016). Like the TLP system most of the restoring loads are generated by line elasticity. As a result, the lines are inclined, and the anchor experiences horizontal and vertical loads. The mooring system comprises 12 polyester mooring lines distributed in two clusters of lines positioned at 60° angles (see Fig. 3d).

The mooring lines are attached at two heights, one at the bottom of the floater with an angle of attachment of 19° and one 10 m below SWL with an angle of attachment of 30° to give sufficient clearance with regards to the fairlead location and free surface and manoeuvring of vessels near the platform. Two sets of the TLB system fairleads are located at 10 m and 52 m below the SWL and have a radius of 6.25 m from the platform centreline. At a depth of 110 m below, the SWL anchors are located along a radius of 180 m from the centreline. The lines are assumed to be steel wire rope
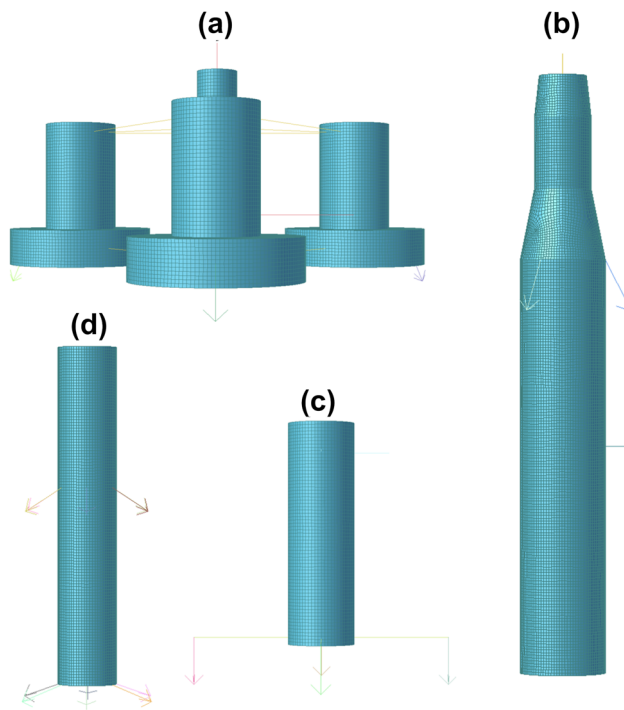
Fig. 5 Mesh converged resolution of Semi-submersible (**a**), Spar (**b**), TLP (**c**), and TLB (**d**) platforms

with a diameter of 0.24 m with 2.33E+09 N axial stiffness having an equivalent mass per unit length of 222 kg/m in air and 177 kg/m in water. BRIDON BEKAERT (2020) provided the data for steel wire rope. ACTEON (2021) provided data for the R5 studdles mooring chain. The mooring system characteristic for each platform is illustrated in Table 2.

3 Methodology and numerical analysis

Figure 4 shows the methodology and flowchart for the numerical simulation. A coupled analysis is applied to investigate the dynamic floater responses in the time domain, considering mooring lines and the wind turbine to capture all dynamic interactions.

In this study, frequency domain and time domain analyses are carried out, focusing on second-order velocity potential. The numerical simulation is based on the potential flow theory. DNV-GL WADAM (Wave Analysis by Diffraction and Morison Theory) is used to conduct the frequency domain hydrodynamic analysis (Veritas 1994). The frequency-domain hydrodynamic analysis is performed without the mooring lines directly; however, the resulting mooring system stiffness is applied to the calculations. Forces and moments are considered in terms of transfer functions. Added mass and radiation damping of hydrodynamic coefficients, wave excitation forces, and response operators are

calculated in WADAM, solved by potential theory based on the implementation of a 3D panel method and Green's theorem in WAMIT (Lee and Newman 2005).

The general equations of motion describing the structure's response are analysed separately for mean, low, and wave frequency responses. The coupled motion response of floating platforms and mooring lines is computed in the time domain in SIMA to provide the dynamic response regarding motion and mooring forces. SIMO considers the linear and potential quadratic forces on the body and Morison's equation for slender parts. The elasticity of slender elements (such as mooring lines) is considered, and the floating structure is assumed rigid. The aerodynamic calculations are performed using the Blade Element Method, considering numerical corrections for stall and wake effects, including dynamic stall and dynamic wake correction. This study also used the external code in TurbSim (Jonkman 2009) to generate the Normal Turbulence Wind (NTM) model for operational conditions and the Extreme Wind Model (EWM) with turbulence intensity for survival conditions.

The most crucial advantage of running a time domain simulation is considering the non-linearities. The step-by-step numerical integration of the incremental dynamic equilibrium equations allows for incorporating these non-linearities. The numerical integration is solved with a Newton–Raphson equilibrium at each time step. The downside of a time domain simulation is that it is time-consuming due to the repeating generation of the stiffness, mass, and damping matrices. The hydrodynamic loading on the elements is computed using 2D strip theory to calculate the hydrodynamic responses from potential flow and the drag term in Morison's equation. The dynamic equilibrium equation is solved in time domain using Newmark-β step-by-step integration. Using a constant time step throughout the simulation. This method uses relation between displacement, velocity, and acceleration at time t and $t + \Delta t$. This paper has utilized the constant average acceleration method with $\gamma = 0.256$ and $\beta = 0.505$, introducing a small amount numerical damping to the simulation. This numerical damping does not provide any significant damping to the system when performing the analyses but avoids numerical instability in the calculations. The time step utilized is 0.005 s, as recommended in SIMA for FOWTs. The constant acceleration method is based on taking the acceleration to be constant in the time step. The boundary value problems will be solved in the following part in both first order and second-order to investigate the hydrodynamic characteristics of the FOWT system. When a platform is not fixed, the first-order motion affects the second-order solution. By considering the quadratic interaction of the two linear wave components of the frequencies ω_i and ω_j, the second-order velocity potential, $\Phi^{(2)}(x, y, z, t)$ which is decomposed into sum $(\omega_i + \omega_j)$ and different $(\omega_i - \omega_j)$ frequency terms where

Table 3 Mesh size converged and element number

Platform	Mesh size (m)	Element no
TLB	0.6	3200
Spar	0.5	5459
TLP	0.7	4992
Semi-Submersible	0.7	51,129

the ϕ_{ij}^{+} and ϕ_{ij}^{-} are referred to the sum and difference frequency.

3.1 Discretization of Platforms

All platforms are modelled in GeniE, a tool for concept (high-level geometry) modelling. The concept model, or parts of it, can be meshed using various finite element types. The influence of different mesh sizes on the performance of each platform was investigated, with Table 3 illustrates the total number of panels and converged mesh size for the support structure is shown in Fig. 5.

Figures 6, 7, 8 and 9 show the influence of different mesh sizes on the performance of each platform type. It should be noted that the bracing and pontoon spokes are not discretised for both the TLP and Semi-submersible platforms since their mass is negligible. In conclusion, mesh resolution was selected to cover all the critical scales in the hydrodynamic computation process. The mesh size options for TLB, Spar, TLP, and Semi-submersible models illustrate in Tables 4, 5, 6, and 7, respectively. It should be noted that symmetry was used in all models but the Semi-submersible. The influence of different mesh sizes on the result of the motion response of the TLB platform for surge, heave, and pitch motions (left side) and forces (right side) is shown in Fig. 6. The system motion responses have reached the stabilised peak amplitude by the mesh size of 0.6 m and less. Hence, based on the mesh convergence study, the final panel model of the TLB floating structure is indicated in red colour in Table 4. The panel model consists of 3200 elements per quarter (12,800 total element numbers by having 0.6 m element size) to reduce computational cost due to symmetric configuration.

Similarly, for Spar, Semi-submersible, and TLP, the influence of different mesh sizes on motion response and forces is investigated. Table 5 illustrates the options considered for investigating the influence of different mesh sizes on the result of the motion response of the Spar platform. The results of the mesh convergence of the Spar shown in Fig. 7 indicate that the system motion responses have reached the stabilised peak amplitude by the mesh size of 0.5 m and less. The final panel model of the Spar floating structure consists of 5459 elements per quarter (21,836 total element numbers by having 0.5 m element size). Table 6 presents the options for

investigating the effect of different mesh sizes on the motion responses for the TLP panel model. The results of TLP mesh convergence shown in Fig. 8 indicate that the TLP panel model reached the stabilised peak amplitude by the mesh size of 0.7 m and less. The final panel model of the TLP platform consists of 4992 elements per quarter (19,968 total element numbers by having 0.7 m element size). The panel model of the complete Semi-submersible floating structure modelled with seven different mesh sizes illustrate in Table 7. Investigating the influence of different mesh sizes on the result of motion responses of the Semi-submersible platform shown in Fig. 9 indicates that the model is converged by 0.7 m mesh size. The final panel model of the Semi-submersible floating structure consists of 51,129 total element numbers.

3.2 Software Verification and Validation

The properties of platforms were modelled and run against available data sets to verify and validate the methodology process. The comprehensive validation for the TLB platform is carried out by Ramzanpoor et al. (2023). The software verification and model validation of the Semi-submersible, Spar, and TLP platforms present in the following.

3.2.1 Spar

Software validation for the Spar platform was carried out by considering the OC3-Hywind Spar buoy (Jonkman 2010a, b) due to the data being openly accessible. The comparison of the hydrodynamic wave excitations from linear diffraction is shown in Fig. 10. The hydrodynamic damping matrices from the linear radiation problem for modes of motion of the platform are shown as a function of oscillation frequency in Fig. 11. It can see that the shape and magnitude of the results achieved from SESAM software are similar to the results obtained from the Jonkman study (Jonkman 2010a, b). The dotted lines are the outcome of the results of SESAM simulations.

3.2.2 Semi-submersible

The SESAM software is used to validate the Semi-submersible system to test against published results from George (2014). George evaluated the platform behaviour of a scaled-up Semi-submersible 10 MW wind turbine compared to a floating 5 MW system. The George study simulated the model using FAST 8. The turbulent wind flow files were generated using TurbSim. Stochastic inflow turbulence code and the computations of WAMIT are applied to provide inputs for the HydroDyn module of FAST.

The structural properties of a 10 MW reduced draft scaled Semi-submersible, including mass, COG, COB, and inertia, are very close to that of George's designed platform. Three
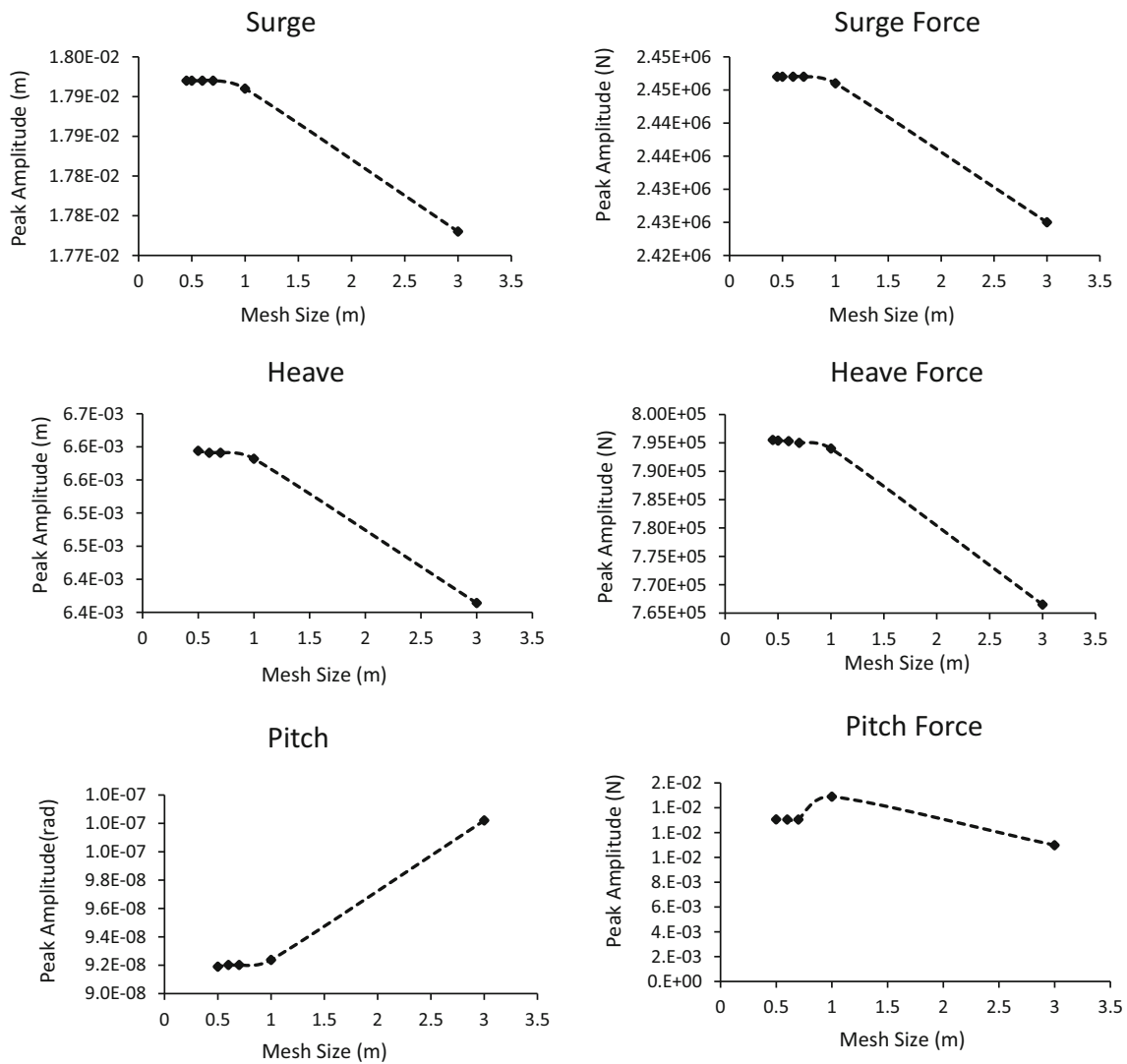
Fig. 6 TLB platform motion response mesh convergence

studdles chain mooring lines are used to fix the FOWT to the seabed. The diameter of the mooring line is 107 mm, with a weight of 229 kg/m. Free decay tests are considered to verify the validation. The comparison of the pitch, heave, and surge motion responses is shown in Figs. 12, 13 and 14.

Comparing the pitch and heave motion responses in Figs. 12 and 13 showed that the SESAM model's amplitude is minimally higher than the George model. This may be due to the same reasons outlined above for the differences in the surge response motions. Figure 14 shows the agreement of results between both cases being excellent across the responses for which data was available. Although the damping is similar, the model simulated in SESAM has approximately ~ 7% greater surge amplitude than the George model. This could be due to weight differences between the SESAM and the George model, as the George model

is slightly heavier. However, this weight variance could be due to differences in the discretisation of the model.

3.2.3 TLP

This study considered the NREL 5 MW wind turbine and MIT/NREL TLP HydroDyn input files (Jonkman 2010a, b; Matha 2010) to validate the process and set up a simulation case for the TLP platform. The excitation forces and moments concerning phase angles from incident waves in the surge direction are shown in Figs. 15 and 16. The calculations are based on the diffraction potential by applying the total wave excitation force. The full excitation force is more conveniently presented in complex form using frequency domain analysis, as described by DNV-OS-J101 (Faltinsen 1993). The magnitude and shape of the results are identical, but the peak magnitude of the surge motion obtained from
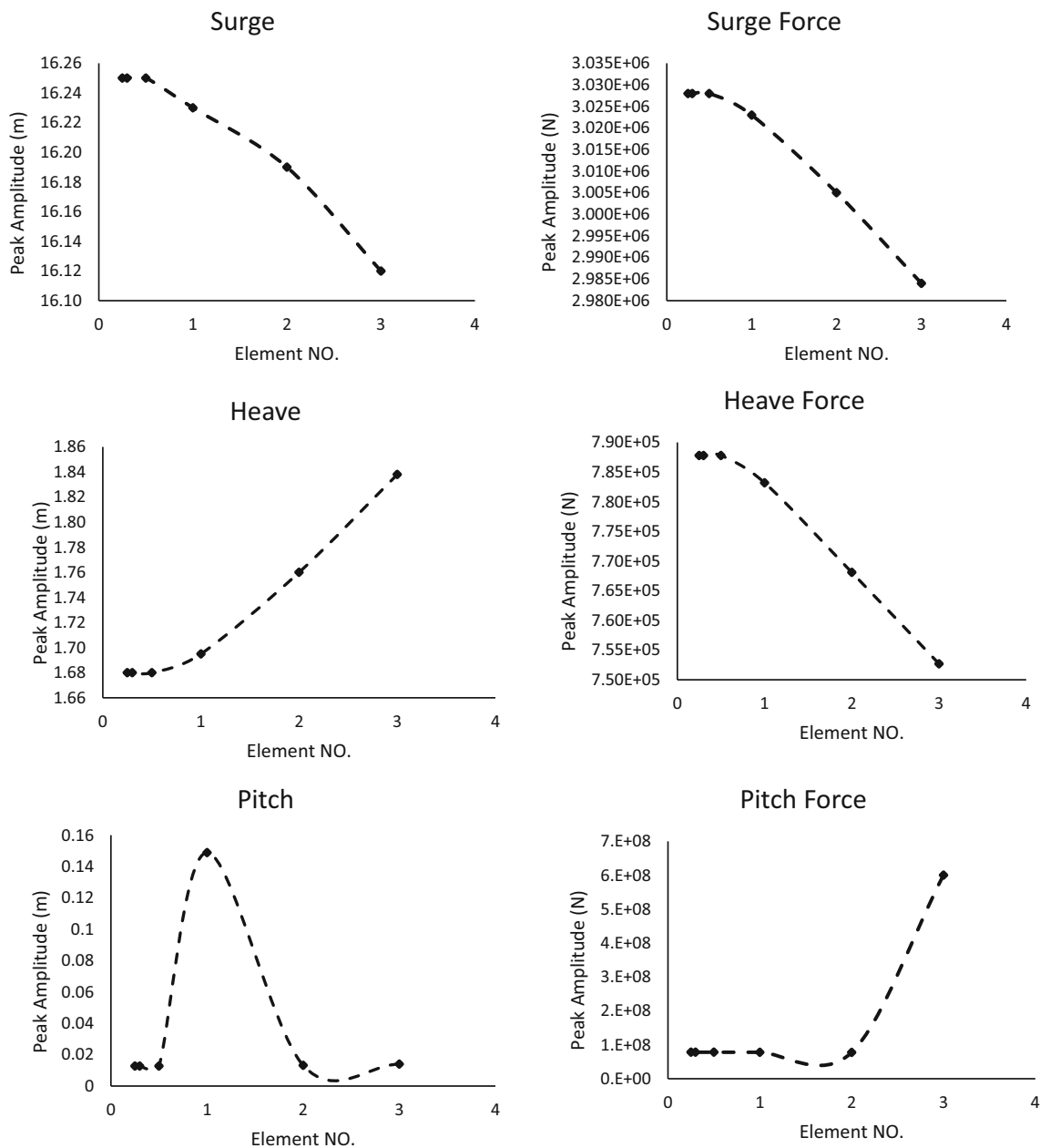
Fig. 7 Spar platform motion response mesh convergence

the SESAM simulation occurred earlier than the MIT/NREL TLP model.

The results of both studies have the same shape and agree very well throughout. The slight difference observed in Figs. 15 and 16 could either be due to the mass matrix input file or could be due to differences in the discretisation of the model within the Matha study (Matha et al. 2010). Figures 17, 18 and 19 compare the results from MIT/NREL TLP HyroDyn input damping coefficients. The results show a similar trend with a slight phase difference. The magnitude

of the damping coefficient in heave is close to zero because of the value of the draft.

By overviewing the results comparison for all platforms, this section has shown excellent agreement of SESAM modelling to the studies across all platform designs, validating the approach for further benchmark testing.
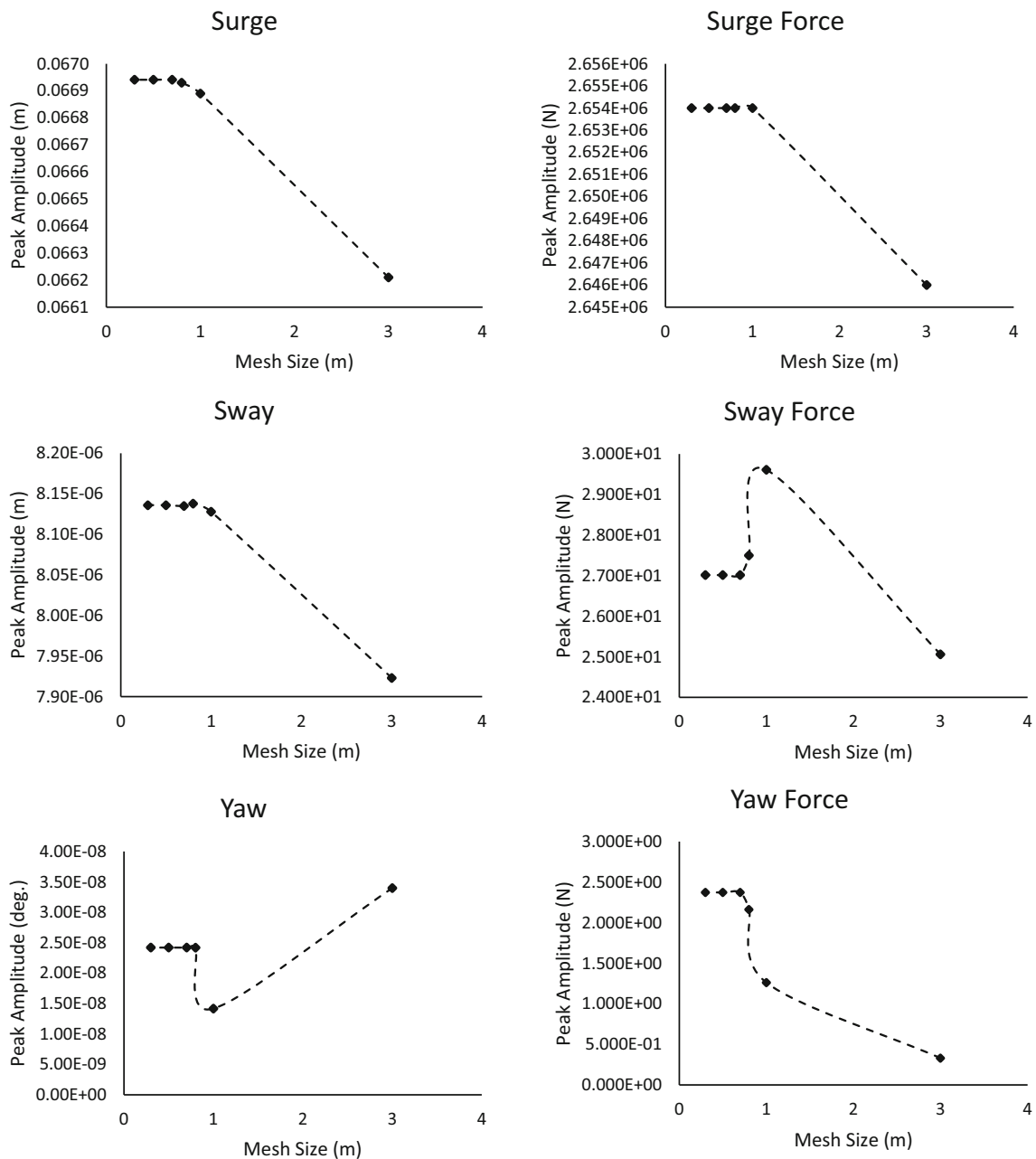
Fig. 8 Semi-Submersible platform motion response mesh convergence

4 Environmental conditions

For specific design of the floater operational area, pre-defined design load cases (DLCs) are required to benchmark response and performance characteristics. The platforms are expected to be deployed in the Northern North Sea, with a water depth of 110 m. For this location, the DNVGL design standard specifies several DLCs (Veritas 2013). Considering all the load cases prescribed by the design standard for this preliminary load analysis is unnecessary. Instead, this study aims to benchmark the TLB and compare it with three platforms

by utilising the ultimate load type during survival and operational conditions. Therefore, four combined environmental load cases are defined for this study, as shown in Table 8 based on DNV-OS-J101 (Veritas 2004), with these DLCs representing operational and survival conditions. The combined design load cases descriptions are shown in Table 8.

Wind conditions are considered using two sets of wind models according to international standard IEC 61400–1 (Madsen and Risø 2008), which are Normal Turbulence Model (NTM) and Extreme Wind Model (EWM). Created
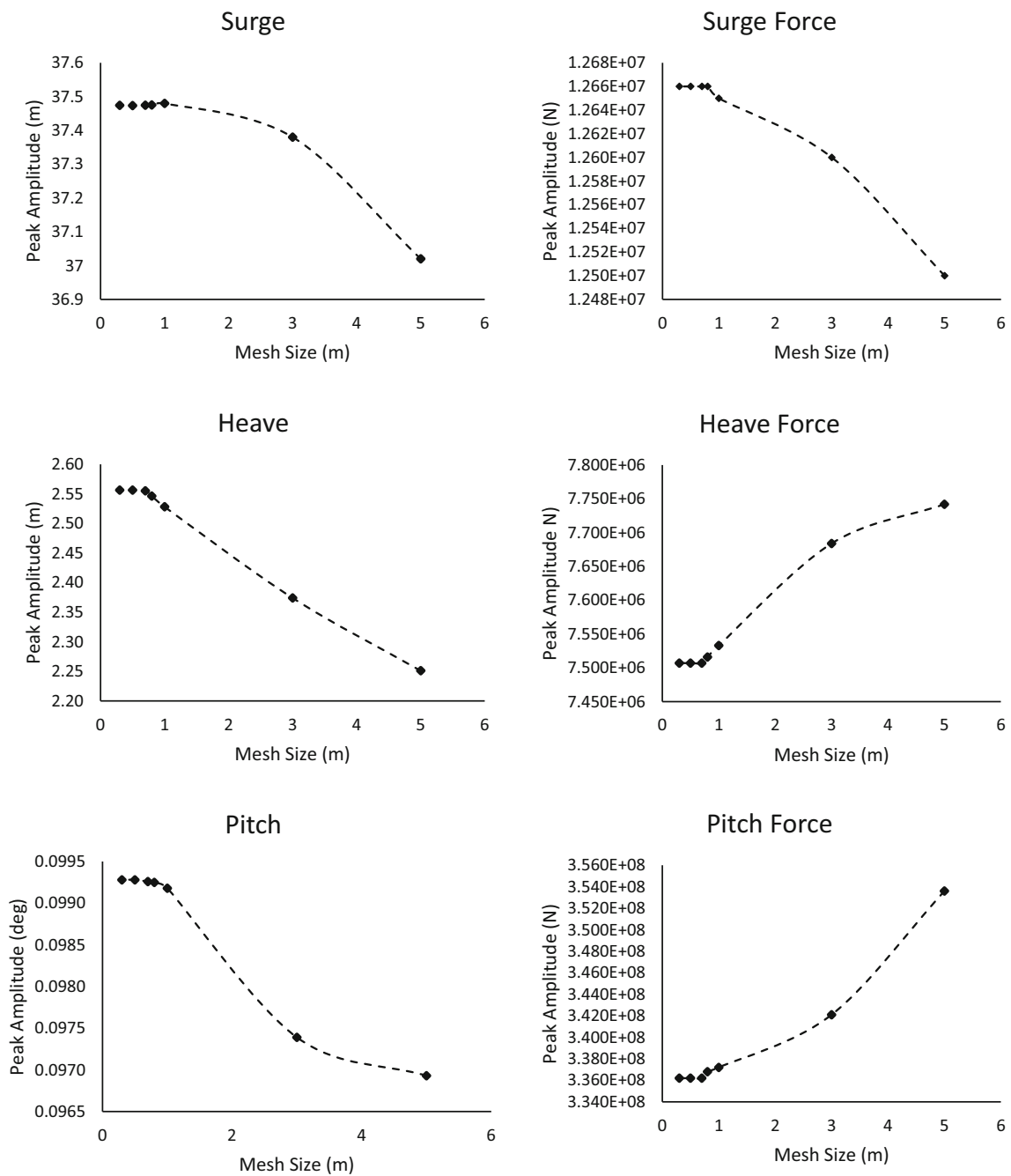
Fig. 9 TLP platform motion response mesh convergence

Table 4 TLB model mesh options

Mesh size (m)	3	1	0.7	**0.6**	0.5	0.45
Element no/quarter	113	1009	2182	**3200**	4482	5537

Table 5 Spar model mesh options	Mesh size (m)		3	2	1	**0.5**	0.3	0.25
	Element no/quarter		176	410	1314	**5459**	15,262	21,790

Table 6 TLP model mesh options	Mesh size (m)	5	3	1	0.8	**0.7**	0.5	0.3
	Element no	5564	10,534	26,852	45,653	**51,129**	88,235	124,501

Table 7 Semi-sub model mesh options	Mesh size (m)		3	1	0.8	**0.7**	0.5	0.3
	Element no/quarter		93	832	3665	**4992**	6015	8466

these models with the TurbSim [59] two NTM representing two operational condition wind scenarios, one at V_{hub} = 11.4 m/s (rated wind speed), and one at V_{hub} = 18 m/s, both within the operational window of the turbine. On the other hand, coded two EWM in TurbSim, one with turbulence and one with steady wind, represent the wind profile for survival conditions. The wind velocity for survival conditions is based on DNV-OS-J103, Appendix B (Regional Environmental Data) (Veritas 2013).

Wave conditions and kinematics have been derived based on northern North Sea data, provided in Appendix B Table B-1 DNV-OS-J103 (Veritas 2013). The significant wave height in 3 h stationary sea state for a return period of 50 years is calculated for DLCs according to DNV rules and regulation, apart from DLC1.1, where the wave heights were calculated based on wind-generated according to the formula provided in Sugianto et al. (2017). The average period was calculated based on DNV-RP-C205 (Veritas 2010). Irregular waves represent certain sea state conditions that are modelled based on spectra for sea surface elevations. The JONSWAP spectrum for developing sea states is used for a peakedness factor of

γ = 3.3. To represent the current in the North Sea, consider both surface tidal current, U_{tide}, and wind-generated current, $U_{wind.}$. The maximum surface tidal current estimation varies from 0.25 to 1.5 m/s over much of the northern North Sea (Vindenes et al. 2018). The current velocity at different heights for the current generated by wind and tidal current for a 50-year return period is calculated based on the formula provided by DNV-OS-J103 (Veritas 2013). Wind, wave, and current loads calculation are illustrated in Table 9.

5 Results

The free decay tests were performed to document the natural period of the system in all six degrees of freedom using the base floater design and applying initial displacement in all translational and rotational motions through specified forces at the beginning of the time domain simulations.

The natural period and damping ratio of platforms are calculated from free decay test as illustrate in Table 10.

Three hours of time-domain simulations are carried out to provide numerical results for four FOWT platforms under all
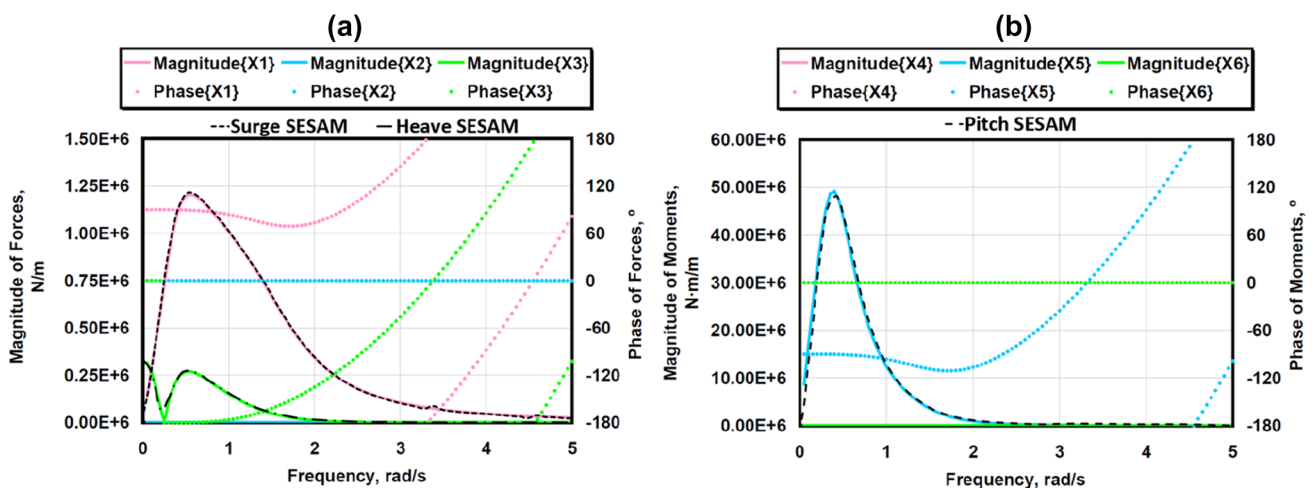

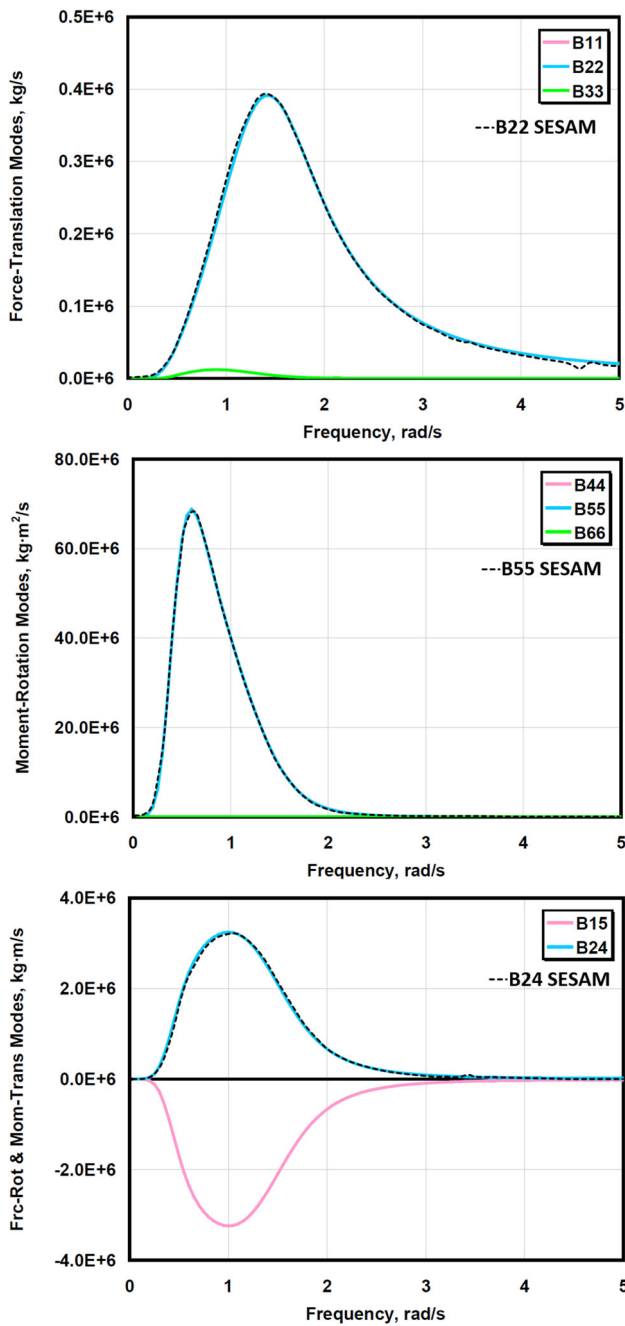**Fig. 10** **a** Transitional and **b** rotational forces per unit amplitude
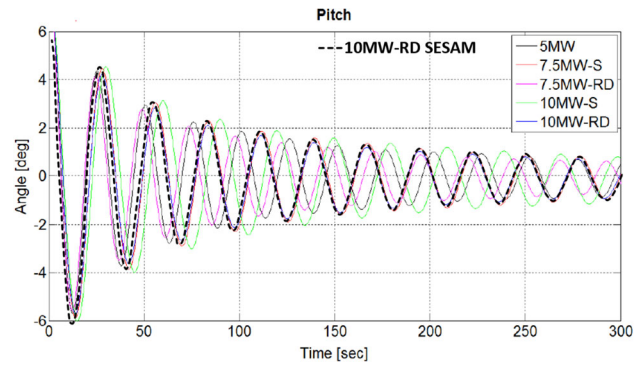
Fig. 11 Hydrodynamics damping comparison

Fig. 12 Pitch motion response comparison
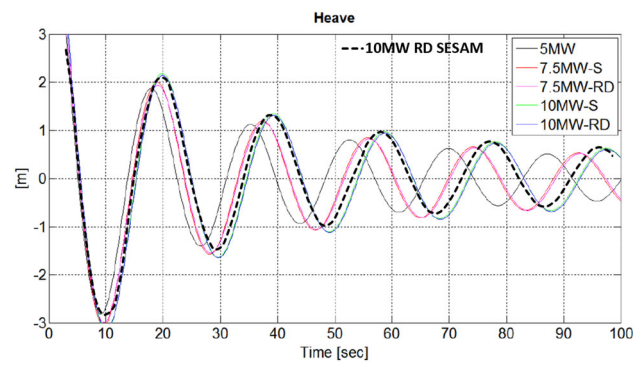
Fig. 13 Heave motion response comparison

Fig. 14 Surge motion response comparison

defined DLCs (see Tables 8 and 9). The results are presented and discussed in terms of the motion and the dynamic tension responses.

5.1 Operational Condition (Power Production)
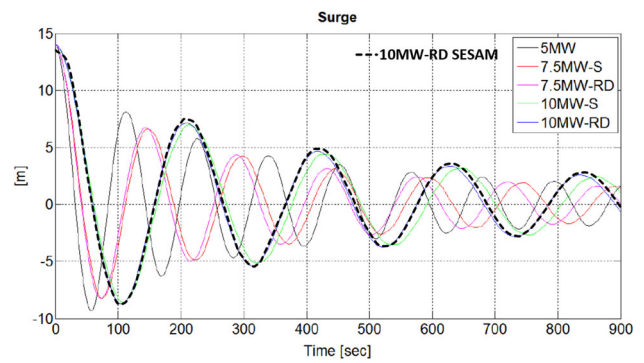
DLC1.1 signifies Normal Sea State (NSS), and DLC1.6a implies Severe Sea State (SSS) to investigate the FOWTs performance during the power production state. The primary objective of selecting two operational conditions is to investigate the environmental limitations of the floating offshore wind turbines' ability to operate. Table 11 presented the summary statistics of motion responses and maximum tension of the maximum loaded line for Semi-submersible, Spar, TLP, and TLB platforms under DLC1.1 and DLC1.6a. The absolute value or magnitude is considered to represent the maximum response.

Comparing the Semi-submersible platform with the Spar under DLC1.1 shows it had increased response by 20% in surge, 54% in sway, 19% in heave, and 21% in yaw motion

Table 8 Combined environmental load cases

|	DLC	Wind	Wave	Current
Power production (operational)	1.1	Normal turbulence model (NTM) $V_{in} < U_{10, Hub} < V_{out}$	Normal sea state (NSS) $H_s = H_S$ at $U_{10, Hub}$	Wind Generated Current
	1.6a	Normal turbulence model (NTM) $V_{in} < U_{10,Hub} < V_{out}$	Severe Sea State (SSS) $H_s = H_{S,50yr}$	Wind Generated Current
Parked (idling) (survival)	6.1a	Extreme wind model (EWM) Turbulent wind $U_{10,Hub}$	Extreme Sea State (ESS) $H_s = H_{S,50yr}$	V_{50yr}
	6.2b	Extreme wind model (EWM) steady wind $U_{10,Hub}$	Extreme sea state (ESS) $Hs = H_{S,50yr}$	V_{50yr}
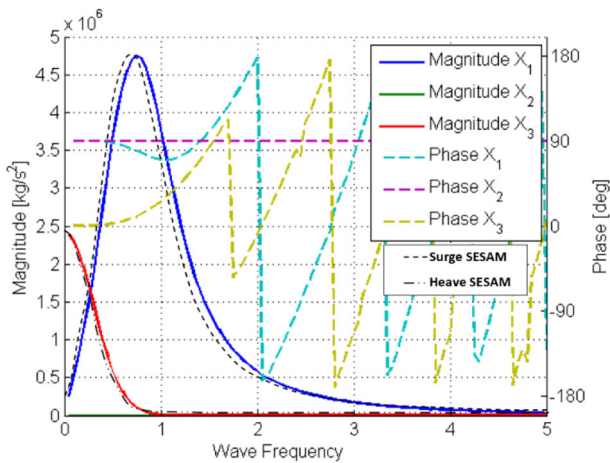
Fig. 15 Force modes of TLP hydrodynamic excitation force coefficients for $\beta = 0°$
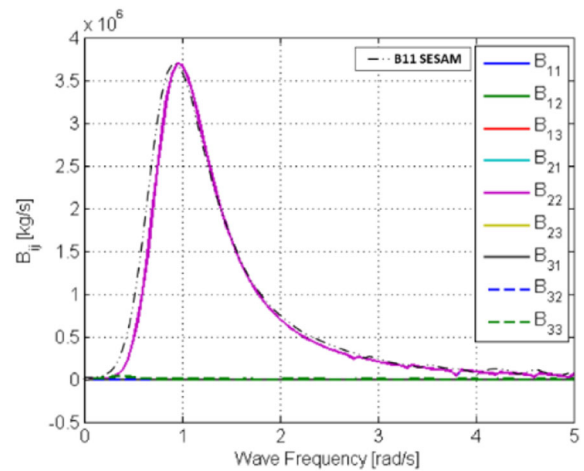

Fig. 17 Force rotation modes damping coefficients
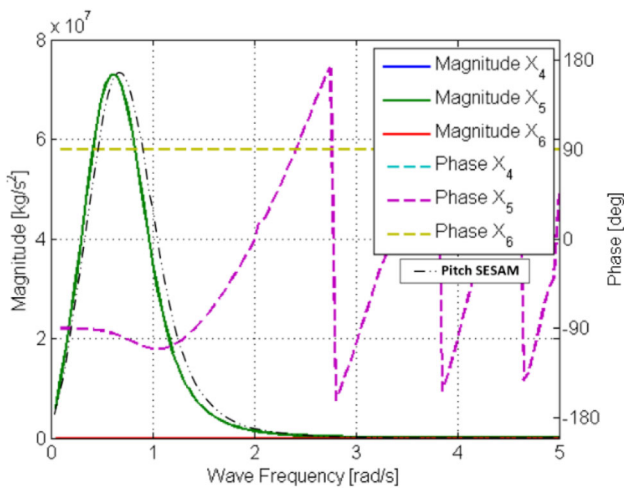

Fig. 16 Moment modes of TLP hydrodynamic excitation force coefficients for $\beta = 0°$
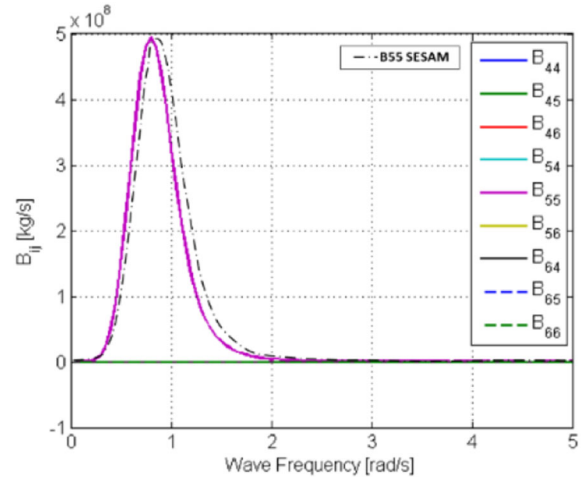

Fig. 18 Moment translation modes damping coefficients

response while the Spar platform experienced higher roll and pitch responses by 43% and 54%. Similar trends are present comparing the TLB and TLP responses. The TLP platform recorded 71% increase in surge, 72% in sway, and 24% in yaw compared to the TLB, while the TLB platform showed higher heave, roll and pitch responses than the TLP platform by 80%, 50%, and 50%, respectively.
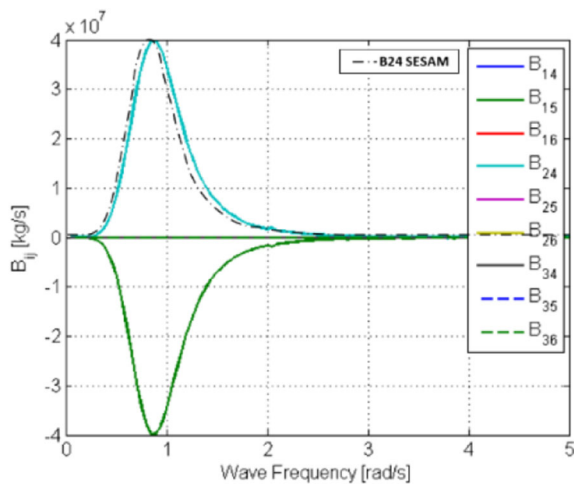
Fig. 19 Force-rotation modes damping coefficients

Analysing the summary statistics of DLC1.6a has shown that the Semi-submersible and TLP surge, heave, and yaw motion responses are coupled with the most loaded line tension. The Spar, surge, heave and dynamic tension of the most loaded mooring line are strongly coupled and dependent on environmental conditions with significant increases seen between normal and severe sea state load cases. Comparing the Semi-submersible platform with Spar under DLC1.6a recognizes it had increased response by 31% in surge, 12% in

sway, 54% in heave, and 18% in yaw response while the Spar had 13% roll and 57% pitch responses higher. Similarly, the TLP had increased response by 43% in surge, 76% in sway, 56% in heave, and 69% in yaw compared to the TLB, whilst the TLB experienced higher roll and pitch responses by 53% and 9%. The maximum set-down heave for the TLP platform occurred due to its surge offset. The Semi-submersible platform recorded higher motion responses in both DLCs than the Spar platform except for roll and pitch motion responses due to the existence of multiple columns and pontoons for Semi-submersible to achieve stability compared with a buoyant cylinder with a deep draft. Apart from surge, the TLP and TLB motion responses are similar under normal sea state conditions. The TLP surge motion response is higher than the TLB, especially in DLC1.6a, while the platform operates in a severe sea state. Due to the TLP platform flexibility design, which is compliant, precluding motions horizontally (surge and sway) and rotationally (yaw) and impact of severe sea state, surge, sway, and yaw motion responses of the TLP platform is higher than those for the TLB platform. As the TLP is designed to be restrained in heave, roll, and pitch, the maximum responses achieved for TLP in such directions are smaller than that for TLB.

The maximum tension presented in Table 10 is for the line that experienced the highest dynamic tension among all

Table 9 Summary of design load combinations

DLC	Wind			Wave			Current
	Model	Speed (m/s)		Model	H_s (m)	T_p (s)	Max speed at SWL (m/s)
1.1	NTM	11.4		NSS	5.2	9.3	$U_{\text{Wind, 50yr}} = 0.442$
1.6a		18		SSS	8.8	12.1	
6.1a	EWM turbulence	51.6		ESS	16.8	16.6	$U_{\text{Tidel, 50yr}} = 1.42$
6.2a	EMW steady	51.6		ESS	16.8	16.6	

Table 10 Natural frequency (rad/s) and damping ratio

Platforms	Surge	Sway	Heave	Roll	Pitch	Yaw
Natural frequency (rad/s)						
Semi-Submersible	0.0091	0.0088	0.3142	0.0571	0.0582	0.2992
Spar	0.0332	0.0269	0.1142	0.1122	0.1102	3.1416
TLP	0.0757	0.0731	2.0944	1.5708	1.5708	0.4833
TLB	0.7854	0.7854	1.2566	0.7854	0.8976	1.2566
Damping ratio						
Semi-Submersible	0.0809	0.1373	0.0571	0.0719	0.0719	0.1180
Spar	0.0332	0.0269	0.1142	0.1122	0.1102	3.1416
TLP	0.0234	0.0232	0.0191	0.0704	0.0704	0.0261
TLB	0.0095	0.0098	0.0901	0.0232	0.0244	0.0435

Table 11 Motions responses and maximum loaded line tension characteristics summary statistics of Semi-submersible, Spar, TLP, and TLB Platforms under DLC1.1 & DLC1.6a events

	DLC1.1					DLC1.6a				
	Time (s)	Max	Min	Mean	Std dev	Time (s)	Max	Min	Mean	Std dev
Semi-Submersible										
Surge (m)	8050	73.1	64.7	68.9	1.4	6776	106.9	0	93.7	7.4
Sway (m)	3065	0.8	− 0.7	0	0.3	6756	1.4	− 1.1	0	0.4
Heave (m)	8387	0.7	− 0.6	0	0.2	6773	4.8	− 4.7	− 0.1	1.3
Roll (°)	10,726	0.4	0	0.2	0.1	10,797	1.2	0	0.6	0.3
Pitch (°)	10,791	0.9	0	0.5	0.3	10,653	1.5	0	0.8	0.4
Yaw (°)	10,660	1.6	− 1.3	0.1	0.4	6775	4.6	− 5	− 0.1	1.2
Tension (ton)	8053	155.7	109.1	130.4	6.8	6775	991.7	0.1	285.7	157.7
Spar										
Surge (m)	8043	58.8	56.1	57.1	0.3	6776	74.2	63.6	69.1	1.5
Sway (m)	3423	0.3	− 0.3	0	0.1	6184	1.2	− 1.1	0	0.3
Heave (m)	8042	0.5	− 0.4	0	0.1	6773	2.2	− 2.1	0	0.6
Roll (°)	10,794	0.8	0	0.4	0.2	10,800	1.3	0	0.7	0.4
Pitch (°)	10,797	2	0	1.0	0.6	10,799	3.5	0	1.8	1.0
Yaw (°)	8981	1.1	− 1.3	− 0.3	0.5	6925	4.1	− 3.8	0	1.1
Tension (ton)	8043	130.3	121.9	125.7	1.2	6774	763.7	602.5	672.2	18.9
TLP										
Surge (m)	2487	4.2	− 2.2	0.3	0.8	6776	19.6	− 18.1	0.2	4.9
Sway (m)	2487	0.9	− 1.1	0	0.3	7906	1.5	− 1.8	0	0.5
Heave (m)	2487	0	− 0.1	0	0	6776	0	− 2.3	− 0.2	0.2
Roll (°)	5396	0.1	0	0.1	0	9513	0.3	0	0.2	0.1
Pitch (°)	10,161	0.2	0	0.2	0	9497	0.9	− 0.1	0.6	0.1
Yaw (°)	2487	0.7	− 0.8	0.1	0.2	6776	2.7	− 3.3	0.3	0.9
Tension (ton)	2485	1124.4	1088	1105.2	3.70	6776	2039.6	1142	1412.2	84.1
TLB										
Surge (m)	10,227	1.2	− 0.4	0.5	0.2	10,224	2.2	− 1.2	0.7	0.4
Sway (m)	10,232	0.3	− 0.3	− 0.2	0.1	7683	0.4	− 0.4	− 0.3	0.1
Heave (m)	9678	0.4	− 0.5	− 0.1	0.1	6144	1	− 1.0	0	0.3
Roll (°)	8714	0.2	0	0.2	0.1	7689	0.5	0	0.4	0.1
Pitch (°)	10,794	0.5	0	0.4	0.1	10,794	1	0	0.7	0.3
Yaw (°)	10,438	0.6	− 0.5	− 0.1	0.3	8587	1.0	− 1	− 0.2	0.5
Tension (ton)	10,227	871	509.9	726.7	42.7	10,224	1089.4	499.8	831	73.2

mooring lines in the system. Line eight from the TLB system and line three from Semi-submersible, Spar, and TLP systems recorded the highest dynamic tension for the given environmental loads' direction. These are the mooring lines in line with the coinciding wind, wave and current forces.

Comparing the maximum tension experienced showed that semi sub mooring line forces were 19% and 23% higher in DLC1.1 and DLC1.6a, respectively than those for the Spar platform. Between TLP and TLB, the maximum force was

increased by 23% and 47%, respectively with higher forces recorded in the TLP lines.

The Spar most loaded line maximum dynamic tension is directly related to the maximum surge and heave motion responses. The TLP maximum tension is strongly coupled with the maximum surge, sway, heave, and yaw, coinciding with maximum tension. The surge response and maximum tension occurred concurrently in the TLB. The maximum dynamic tension event of the Semi-submersible occurred 3 s after the platform experienced the maximum surge but at
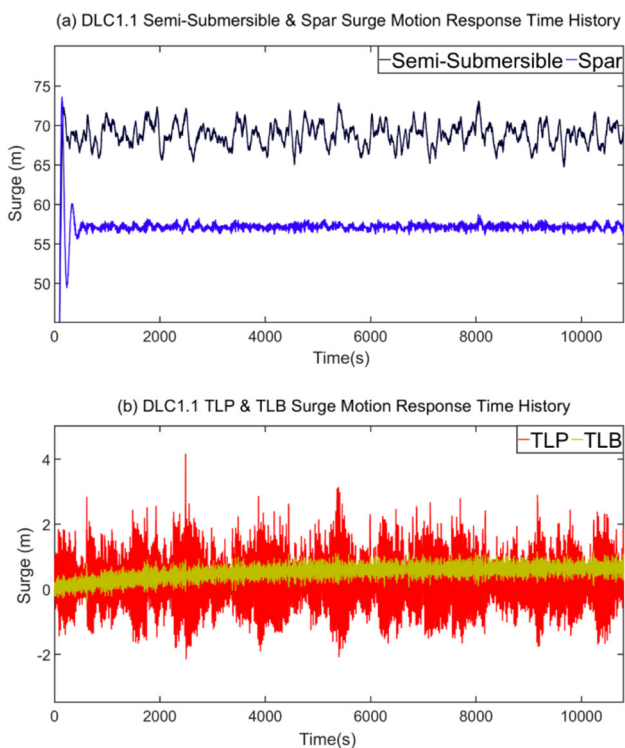
Fig. 20 Time history of surge motion response for Semi-submersible and Spar (**a**) and TLP and TLB (**b**) under DLC1.1 event

Fig. 21 Time history of surge motion response for Semi-submersible and Spar (**a**) and TLP and TLB (**b**) under DLC1.6a event

the same time as maximum yaw. This could be an indication of the complex motion for the Semi-submersible causing increasing tension due to displacement and rotation of a more complex floater structure and missing symmetry.

Figures 20 and 21 show the Semi-submersible and Spar (a) and TLP and TLB (b) surge motion response time history under DLC1.1 and DLC1.6a, respectively.

The platforms with catenary mooring systems have higher surge responses than those with tension mooring systems and show different behaviour of slow-frequency motion compared to the high-frequency motions experienced by the stiff mooring stabilised platforms. The Spar surge response is dominated by high frequency motions, whilst the Semi-submersible shows the combination of lower frequency motion with higher frequency oscillation. The mean line surge response of the Semi-submersible platform is higher than the Spar. On the other hand, the TLB and TLP are dominated by high-frequency motion, whilst the TLP has more oscillation due to the nature of its surge motion; however, the mean surge offset is almost similar. The TLB with stiff mooring characteristics results in low-magnitude motion response at high frequency. By operating in harsh environmental conditions, the magnitude of the surge response increased for all platforms. The platforms with catenary mooring systems have higher frequency oscillation surge response with higher magnitude in operational conditions while exposed to
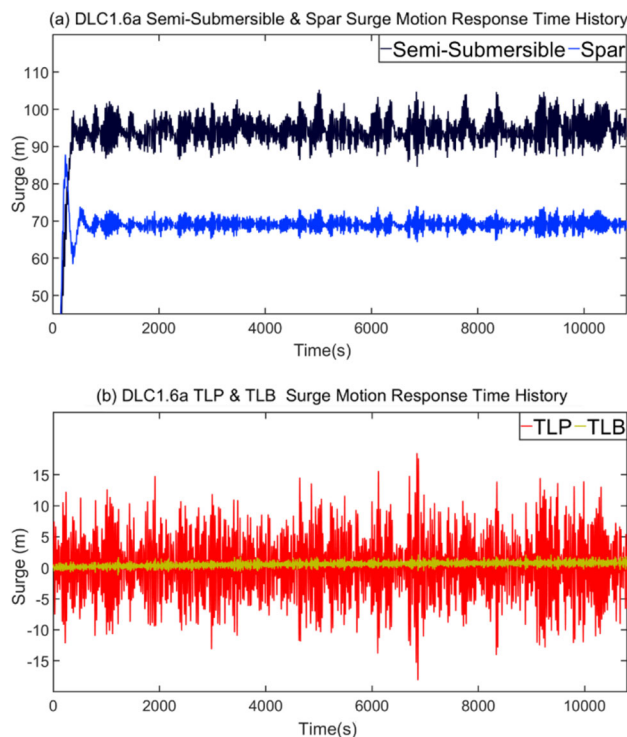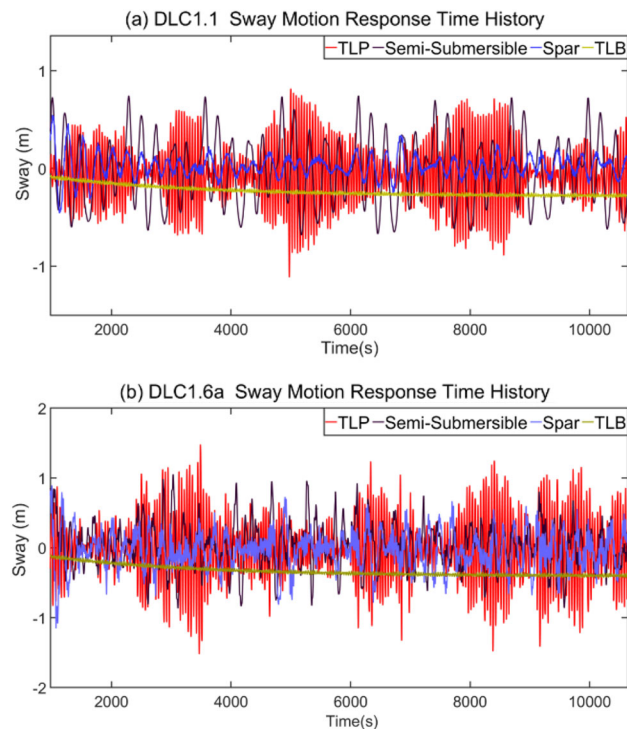

Fig. 22 Time history of sway motion response for Semi-submersible, Spar, TLP, and TLB platforms under DLC1.1 (**a**) and DLC1.6a (**b**) events

(a) DLC1.1 Heave Motion Response Time History

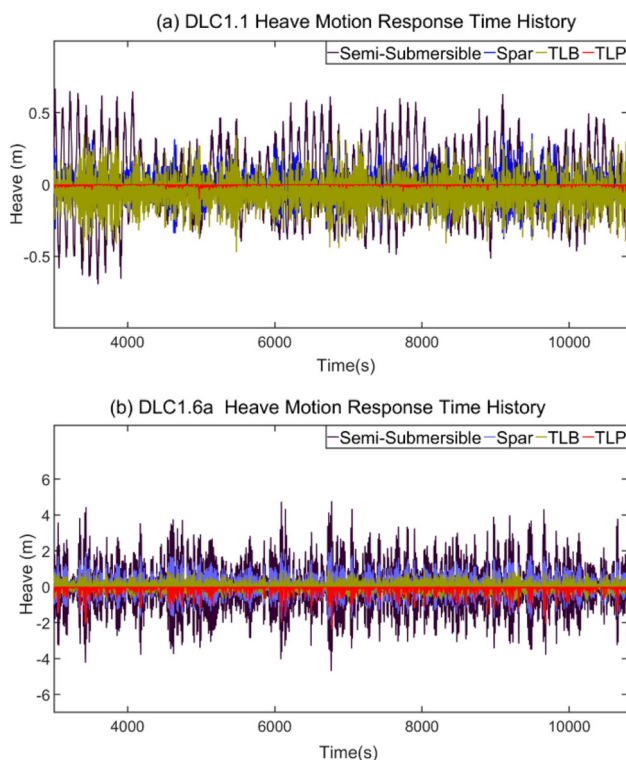(b) DLC1.6a Heave Motion Response Time History

Fig. 23 Time History of Heave Motion Response for Semi-submersible, Spar, TLP, and TLB platforms under DLC1.1 (**a**) and DLC1.6a (**b**) events

harsher environments. The TLP platform has high frequency with elevated magnitude surge response. The TLB system is designed to limit the response motion, whilst the TLP is a complaint design platform in surge direction; however, the mean line surge motion response of both platforms is close together. The platform design characteristics and its mooring system design are essential to platform surge responses.

In terms of sway motion responses, Fig. 22a shows that the maximum sway responses for four platforms under the DLC1.1 event are small and less than a meter. Having a small sway motion response is due to the assumed colinear environmental condition and largely symmetrical design of the platforms. However, the maximum magnitude of sway response obtained for the Semi-submersible and TLP are similar. The TLP platform is compliant in the horizontal motions, which results in more oscillation in the sway direction. The slightest oscillated sway was computed for the TLB platform due to the spread and stiff mooring systems. Figure 22b shows that the TLP has a more fluctuating sway motion response with a higher maximum absolute value than the other platforms. The TLB has the most negligible sway motion response among platforms due to its mooring system physical design characteristics and the collinear directionality of the environmental loads.

Figure 23 shows the heave motion responses of platforms for DLC1.1 (a) and DLC1.6a (b). The Semi-submersible experienced a higher heave motion response due to more water plane area. Moreover, it could depend on the heave plate, which did not assume for the Semi-submersible model in this study. The TLB and TLP platforms oscillate with high frequency with less magnitude in the heave direction compared to platforms with catenary mooring systems due to higher mooring line axial stiffness. The maximum set-down heave for the TLP platform occurred due to its surge offset; the TLP has less heave response than the TLB due to the higher axial stiffness of a larger mooring line diameter. TLP tether is assumed to be vertically secure the platform to the seabed and constructed of a larger and heavier steel wire rope, whilst the taut lines ensure the TLB platform with an angle of attachment to the seabed.

Figure 24 shows the roll motion responses obtained for four platforms under DLC1.1 (a) and DLC1.6a (b) events. The last 400 s of the platform's roll motion response are presented on the right-hand side of Fig. 23. It can be noted that the TLB platform rolled with higher frequency and lower magnitude. The magnitude of the roll motion responses is insignificant under both operational conditions due to the inline wave, wind and current. The platforms with tension mooring systems are seen settling at their rolling mean offset quicker than with catenary mooring systems. The Spar platform follows a linear trend increasing the roll motion with increasing simulation time. Semi-submersible follows a similar trend, although more high-frequency variations can be seen towards the end of the DLC event. The Spar platform has experienced more rolling than the Semi-submersible because the Semi-submersible platform has multiple columns, which means additional restoring moments. On the other hand, TLB converges to a relatively constant roll position throughout the simulation, reaching this state halfway through the simulation. TLP converges faster, showing several low and high-frequency variations around this roll motion angle.

In terms of the pitch motion, Figs. 25 and 26 shows the pitch motion response time history for all platforms under DLC1.1 and DLC 1.6a events, respectively. The pitch response continued to increase for catenary mooring platforms with increasing simulations time, especially for the Spar platform, due to the restoring stiffness in pitch provided by the mooring systems and type of floater. Catenary mooring systems provide little restoring for the pitch motion, whereas the pitch stiffness increases in both tensioned mooring designs. With increasing stiffness, the tendency for high-frequency motions increases. Therefore, the settled pitching means offset occurred quicker because of the platform's structure configuration complexity and mooring system characteristics. The Semi-submersible has less pitching response than the Spar because the Semi-submersible has more columns and achieved stability by the restoring

Fig. 24 Time history of roll motion responses for Semi-submersible, Spar, TLP, and TLB platforms under DLC1.1 (**a**) and DLC1.6a (**b**) events
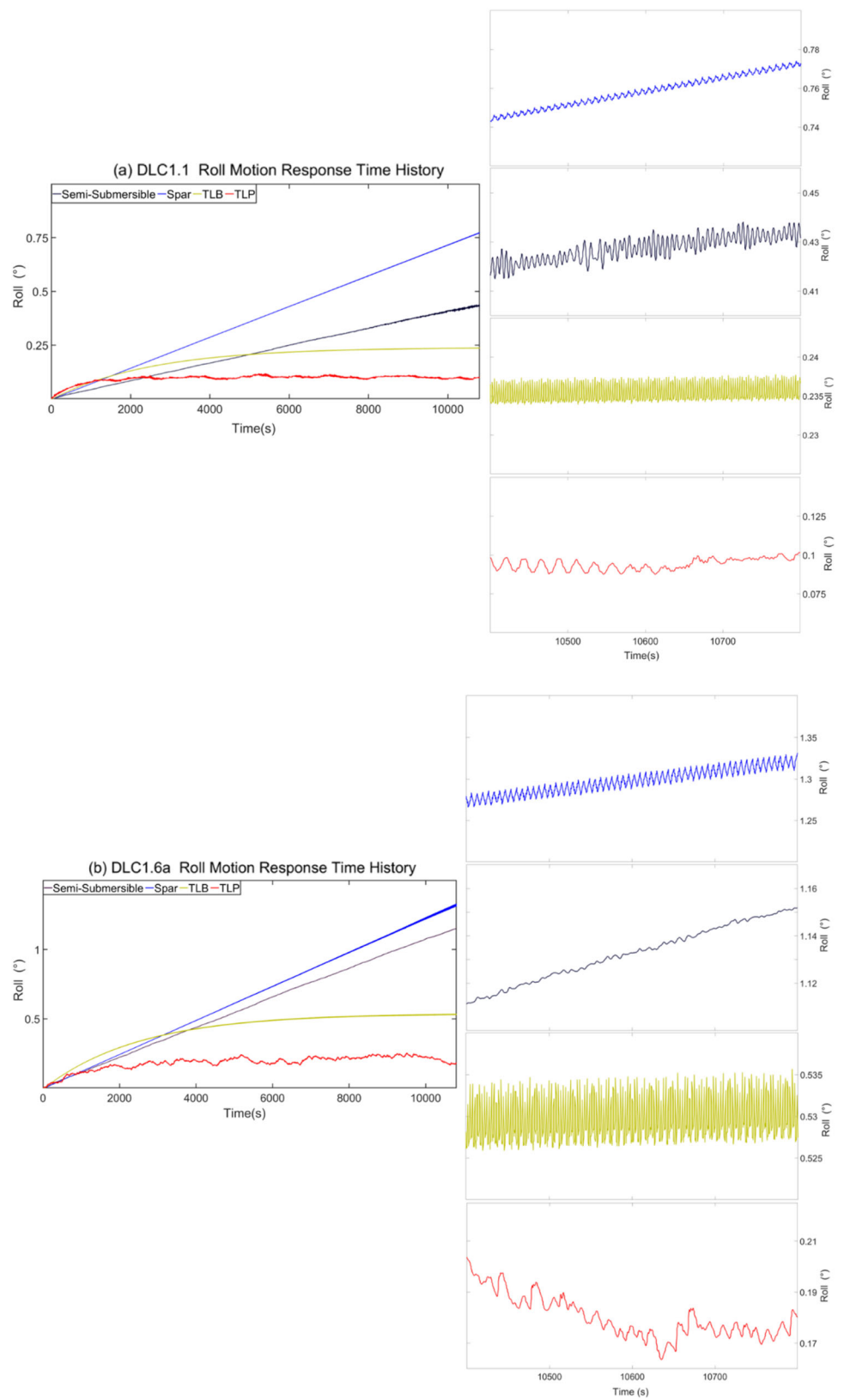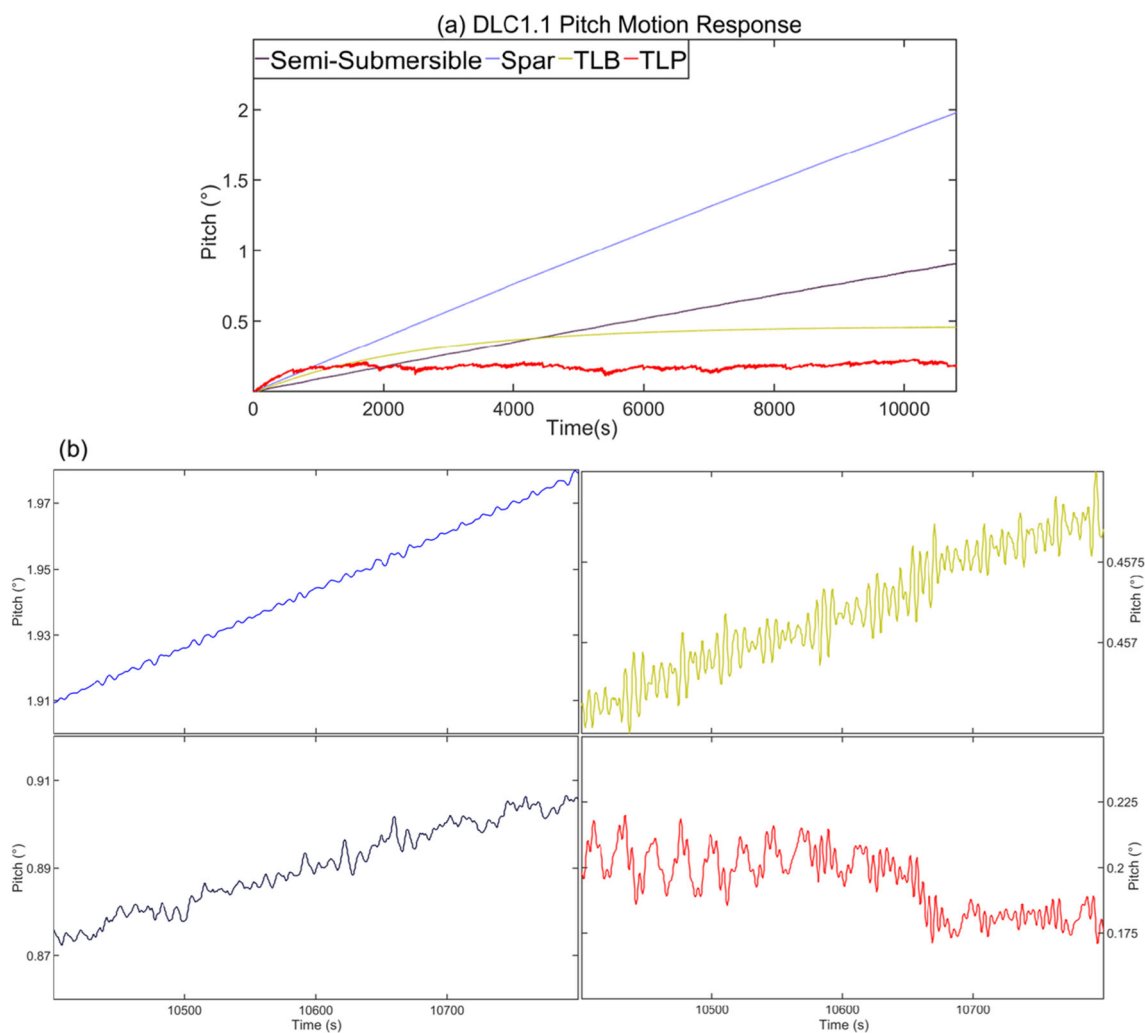
Fig. 25 Full time history of pitch motion responses for Semi-submersible, Spar, TLP, and TLB platforms (**a**) and last 400 s (**b**) under DLC1.1 event

moment of its columns, whilst Spar has a more significant draft, causing a more overturning bending moment.

Figure 27 shows the yaw motion responses of Semi-submersible, Spar, TLP, and TLB platforms under DLC1.1 (a) and DLC1.6a (b). Spar, Semi-submersible and TLB show the very typical behaviour in yaw, albeit at slightly different periods. The Spar and TLB design show periodic behaviour and could be linked to either the natural frequency of the floater or the turbine operation. By comparing Figs. 27a and b, it can be seen that the platform with a catenary mooring system has high-frequency yaw motions while under the harsh environmental condition. The maximum yaw response of the Semi-submersible platform is the highest among other platforms. Structural complexity and shorter mooring lines compared to the less complex Spar structure contribute to this response. Similarly, the TLP platform has slightly more yaw motion than the TLB platform. A possible explanation is that the TLP is compliant in the yaw direction, whilst TLB can assume to be similar to a fixed platform. In addition, the

assumption of a 20° spread of the attachment point for the TLB platform could be influential, whilst it must be adjusted for Semi-submersible and Spar platforms. It should be noted that due to the design characteristics of the TLP platform, a 20° spread of the attachment point did not apply.

Figures 28 and 29 present the time history maximum tension for the line that experienced the highest tension among all mooring lines in the system under DLC1.1 and DLC1.6a, respectively. Line 8 from the TLB system and line 3 from Semi-submersible, Spar, and line 2 for TLP systems recorded the highest tension for the given environmental loads. As it was mentioned earlier, the Semi-submersible surge response and maximum tension of the most loaded line occurred concurrently, whilst the Spar most loaded line maximum dynamic tension is directly related to the maximum surge and heave motion responses due to the colinear environment, catenary mooring system and platform design characteristics. From Fig. 28a, the line representing the mean tension response for the Spar platform is close to that for
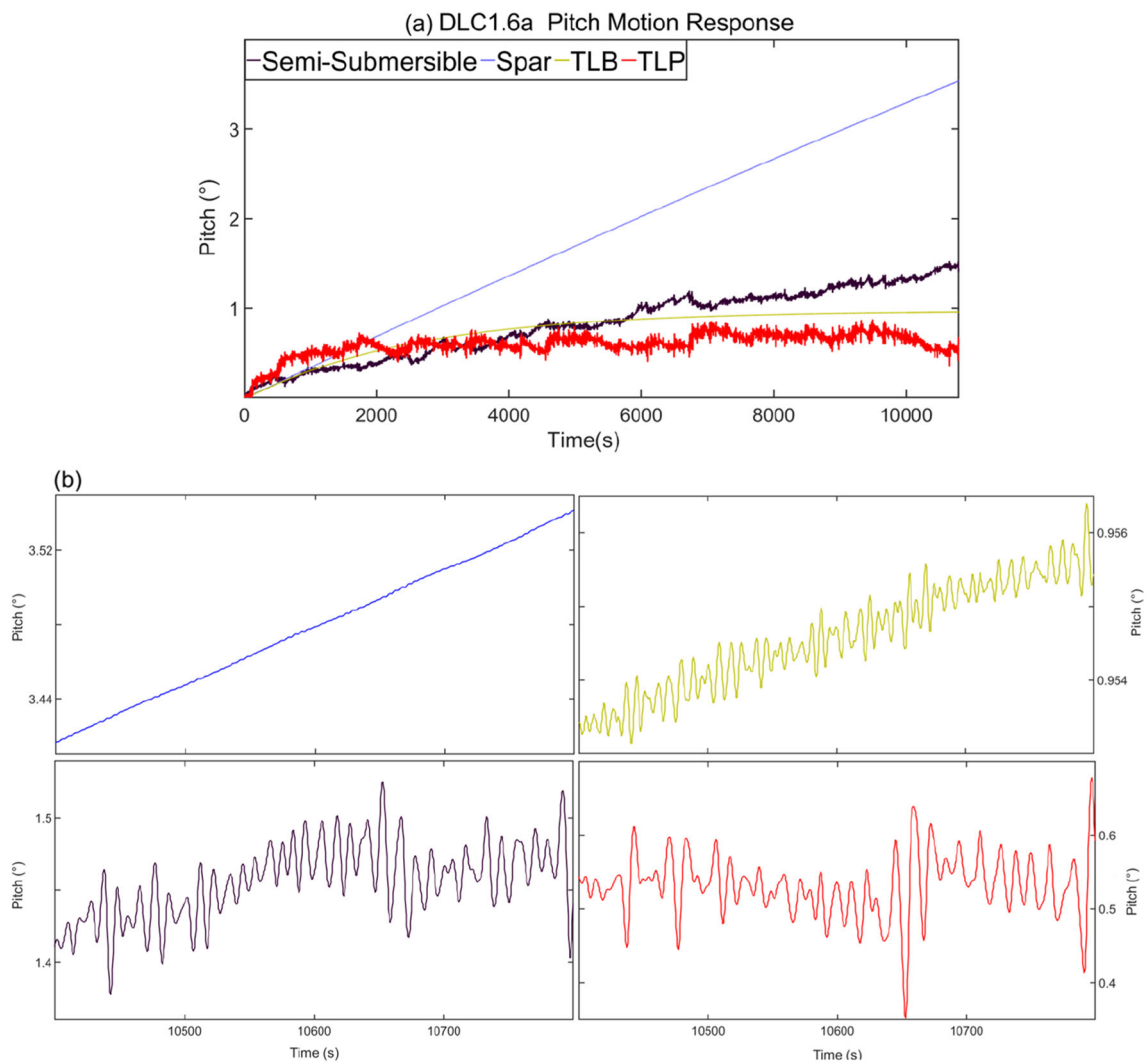
Fig. 26 Full time history of pitch motion responses for Semi-submersible, Spar, TLP, and TLB platforms (**a**) and last 400 s (**b**) under DLC1.6a Event

Semi-submersible. In contrast, the Semi-submersible platform has higher fluctuation from the mean. This means the surge motion of both Semi-submersible and Spar platforms and the dynamic tension of their most loaded mooring line are strongly coupled and dependent on environmental conditions.

The maximum tension carried by the Semi-submersible most loaded line is more than that for the Spar due to experiencing a higher surge by the Semi-submersible platform. Due to the mooring system and platform design characteristics, the TLB surge response and maximum tension of the most loaded line occurred concurrently. Whilst the TLP maximum tension is strongly coupled with the maximum surge, sway, heave, and yaw, all maximums co-occur. Therefore, the TLP most loaded mooring line experienced a higher tension response than that for the TLB platform. Figure 28b shows that the TLB most loaded line experienced more

frequency with higher fluctuations compared to the low frequency higher mean line tension of the TLP most loaded line. The characteristics mooring system and mooring line feature play an essential role. Furthermore, the TLP flexibility in the surge, sway, and yaw directions is another case of higher tension on the mooring line. The TLB mooring system is designed to limit motion responses.

It can be seen from Fig. 29a that the Semi-submersible has higher fluctuation with a higher maximum magnitude than the Spar platform. The Spar platform mean value of the dynamic tension response is higher than for the Semi-submersible because the Semi-submersible due has a smaller mooring line length, which causes more tension on the line. Figure 29b shows that the TLP platform's most loaded mooring line fluctuated more with higher frequency while the platform operated in harsh environmental conditions. The pattern of the most loaded line of the TLB platform is similar

Table 12 Electrical generator output of platforms under DLC1.6a event

Platform	Time (s)	Max (MW)	Min	Mean	SD
Semi-Submersible	61.2	10	5.57	9.46	0.72
Spar	69.9	10	6.90	9.58	0.65
TLP	53.1	10	5.94	9.40	0.75
TLB	53.1	10	8.05	9.70	0.54

Table 13 Motions responses and maximum loaded line tension characteristics summary statistics of Semi-submersible, Spar, TLP, and TLB platforms under survival events

|	DLC6.1a					DLC6.2b				
	Time (s)	Max	Min	Mean	Std dev	Time (s)	Max	Min	Mean	Std dev
Semi-Submersible										
Surge (m)	3431	131.6	0.0	107.6	7.1	3431	124.7	0.0	99.9	7.0
Sway (m)	7455	1.3	− 1.3	0.0	0.6	3018	1.0	− 0.9	0.0	0.3
Heave (m)	3428	5.2	− 5.2	− 0.1	1.4	3428	4.4	− 3.9	− 0.1	1.1
Roll (°)	10,575	1.3	0.0	0.6	0.4	10,792	1.0	0.0	0.5	0.3
Pitch (°)	10,796	3.3	0.0	1.6	1.0	10,796	2.8	0.0	1.3	0.8
Yaw (°)	3428	10.0	− 9.3	− 0.1	2.5	3428	8.3	− 7.7	− 0.1	2.1
Tension (ton)	3430	1682.6	80.35	889.72	154.8	3430	1477.2	54.88	767.23	142.1
Spar										
Surge (m)	6771	107.4	0.1	96.8	5.5	6771	102.9	0.1	92.9	5.1
Sway (m)	9717	1.1	− 0.7	0.0	0.2	6234	1.0	− 0.9	− 0.1	0.2
Heave (m)	6768	2.2	− 2.1	0.1	0.5	6768	1.9	− 1.8	0.1	0.6
Roll (°)	10,799	2.5	0.0	1.3	0.7	10,799	1.9	0.0	1.0	0.5
Pitch (°)	10,795	4.9	0.0	2.5	1.4	10,795	3.7	0.0	1.9	1.0
Yaw (°)	6786	6.2	− 6.4	− 0.6	2.1	6786	5.3	− 5.2	− 0.5	1.7
Tension (ton)	6770	1598	119.7	1199.8	103.7	6770	1506.5	125.1	1107.1	100.2
TLP										
Surge (m)	3432	29.9	− 27.9	0.8	7.1	3432	24.6	− 22.5	1.1	5.9
Sway (m)	8159	2.1	− 2.3	0.0	0.6	6486	1.2	− 1.9	0.0	0.4
Heave (m)	3432	0.1	− 5.3	− 0.3	0.4	3432	0.1	− 5.0	− 0.2	0.4
Roll (°)	8794	0.6	− 0.1	0.2	0.1	1523	0.5	− 0.5	0.0	0.2
Pitch (°)	3436	0.7	0.0	0.6	0.1	3436	0.6	0.0	0.5	0.1
Yaw (°)	3428	4.4	− 4.1	0.0	1.1	3428	3.9	− 3.6	0.0	1.0
Tension (ton)	3431	2548.9	987.6	1516.0	128.8	3431	2286.9	916.5	1305.1	114.7
TLB										
Surge (m)	6094	2.9	− 2.0	0.7	0.6	6094	2.5	− 1.3	0.5	0.5
Sway (m)	8546	1.0	− 0.7	0.0	0.2	8546	0.6	− 0.6	0.0	0.1
Heave (m)	6771	1.4	− 1.6	0.0	0.4	6772	1.4	− 1.5	− 0.1	0.4
Roll (°)	9273	0.3	− 0.9	− 0.3	0.2	9273	0.3	− 0.8	− 0.2	0.2
Pitch (°)	10,796	1.8	0.0	1.3	0.5	10,796	1.5	0.0	1.1	0.4
Yaw (°)	6094	1.0	− 1.6	− 0.1	0.3	6095	0.9	− 1.4	0.0	0.3
Tension (ton)	6094	1448.9	355.3	908.7	147.5	6094	1332.5	338.3	841.4	134.1
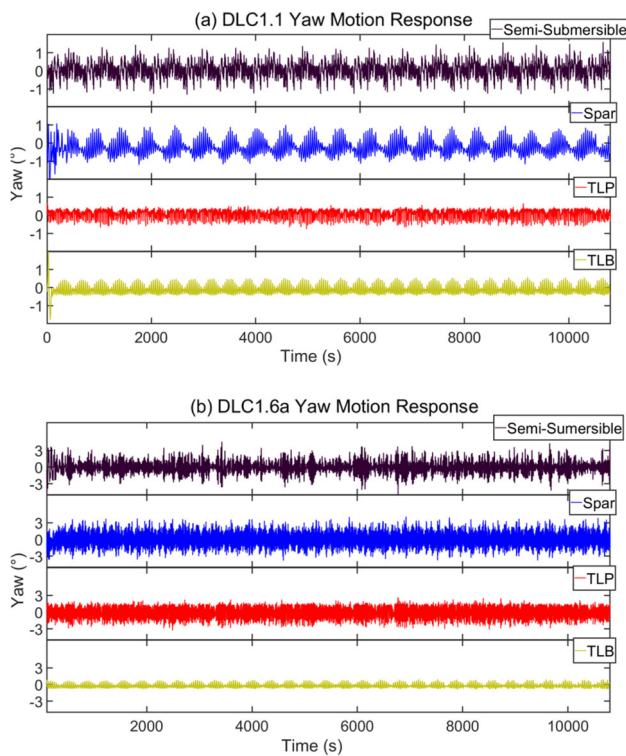
Fig. 27 Time history of yaw motion responses for Semi-submersible, Spar, TLP, and TLB platforms under DLC1.1 (**a**) and DLC1.6a (**b**) events

for both DLC1.1 and DLC1.6a, only with recording higher magnitude with higher mean tension for DLC1.6a.

As the primary focus of this section was to investigate what would be the environmental limitations of the floating offshore wind turbines' ability to operate, in the following the results of electrical generator output of platforms under DLC1.6a event will present.

The power performance of a FOWT depends on system dynamics response under environmental condition and wind turbine control system strategy. A similar wind turbine control system is considered for all platforms. Table 12 illustrates the statistical characteristics of the platforms electrical generating under DLC1.6a. Figure 30 shows the time history of power output generator for four platforms.

As demonstrated by Table 11, however, the average electrical generator output of all platforms is similar, the TLB platform generated slightly more power among other platforms based on the simulation. The lowest power generated from TLB platform within 3 h simulation is 8 MW due to its motion responses.

5.2 Survival condition-parked (idling)

An extreme sea state (ESS) with a significant wave height of 16.8 m represents the survival condition wave model. Two
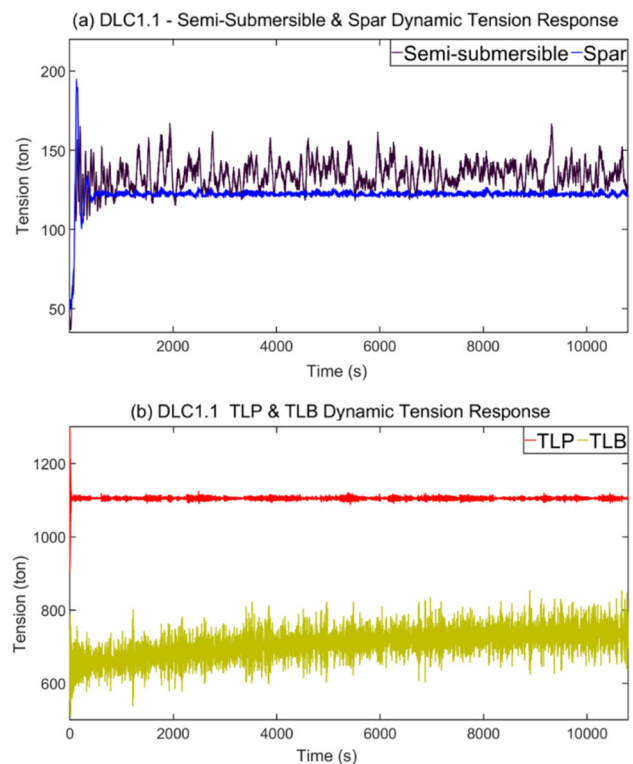
Fig. 28 Loaded line tension response time history for Semi-submersible and Spar (**a**) and TLP and TLB (**b**) platforms under DLC1.1 event
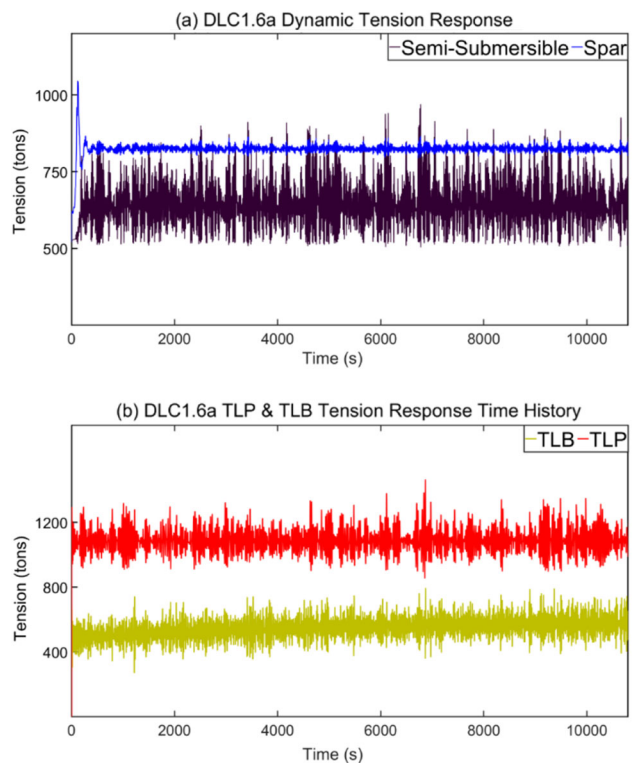

Fig. 29 Loaded line tension response time history for Semi-submersible and Spar (**a**) and TLP and TLB (**b**) platforms under DLC1.6a event
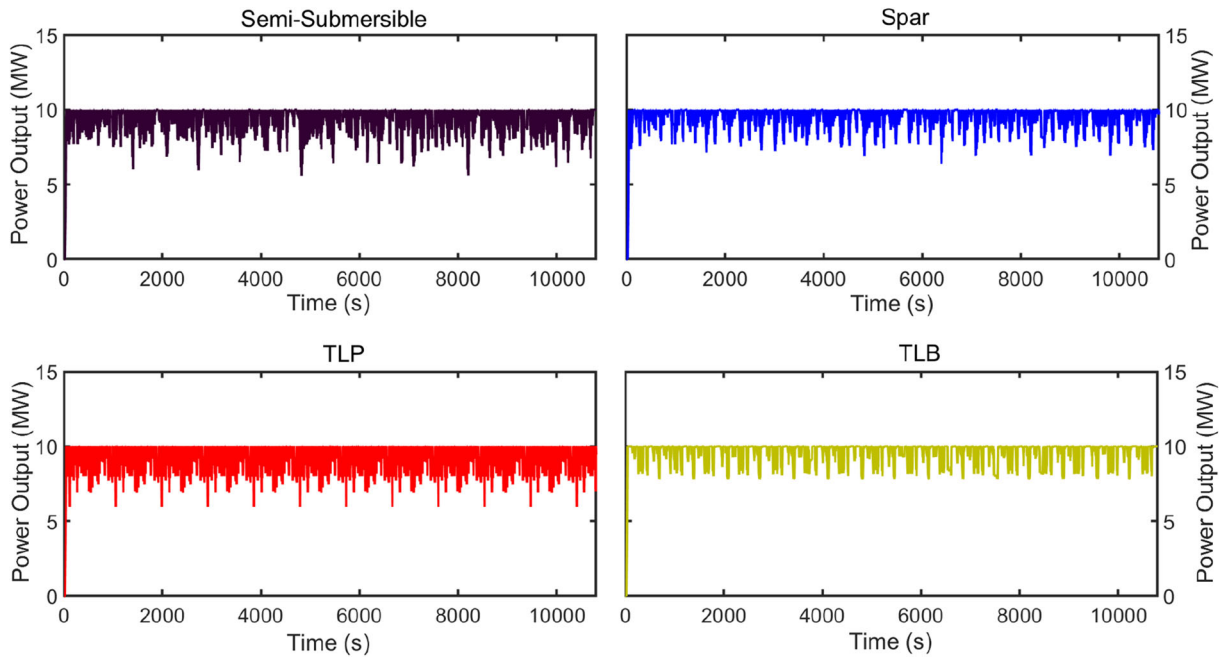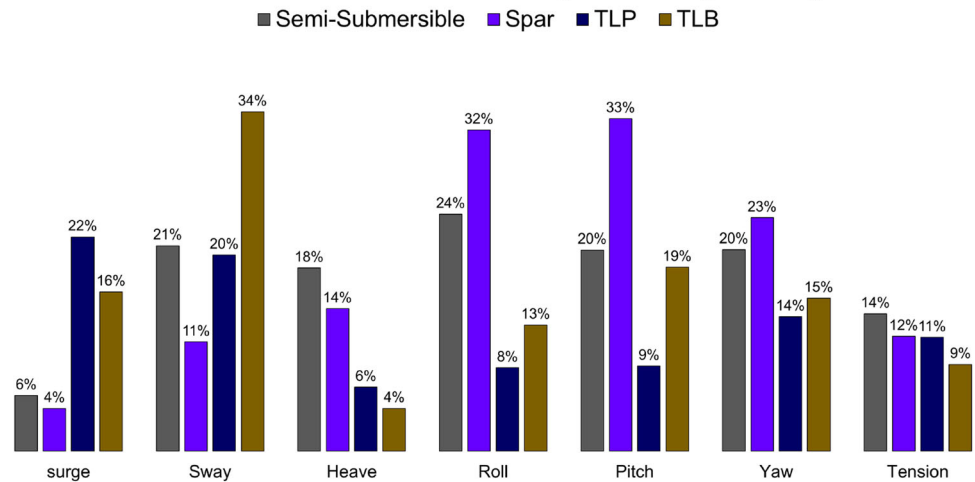
Fig. 30 Power output generator time history of Semi-submersible, Spar, TLP, and TLB platform under DLC1.6a event

Fig. 31 Induced effect of wind turbulence intensity on responses for Semi-submersible, Spar, TLP, and TLB platforms

wind models have been coded in TurbSim to describe the EWM, one with the appearance of turbulence and another with a steady profile. The maximum tidal speed of 1.42 m/s with 50-year return period is assumed for both survival conditions. The primary objective is to investigate the induced effect of the wind turbulence intensity on each platform's motion response performance and maximum dynamic tension on most loaded lines. Table 13 shows motion responses and most loaded line tension summary statistics of Semi-submersible, Spar, TLP, and TLB platforms under survival events with (DLC6.1a) and without (DLC6.2b) wind turbulence.

The Semi-submersible platform has experienced maximum heave and yaw concurrently, followed by achieving maximum surge response (after 3 s) consequence of having maximum dynamic tension under both DLCs. First, the Spar platform recorded maximum heave. Then, the highest maximum dynamic tension of the most loaded line occurred when the maximum surge response occurred, followed by the peak yaw response for both environmental events. The TLP platform underwent extreme yaw response, then experienced maximum surge and heave responses (after 4 s) concurrently, and the consequence recorded maximum dynamic tension under survival conditions. The platform recorded the utmost pitching after 4 s the most loaded line experienced the peak
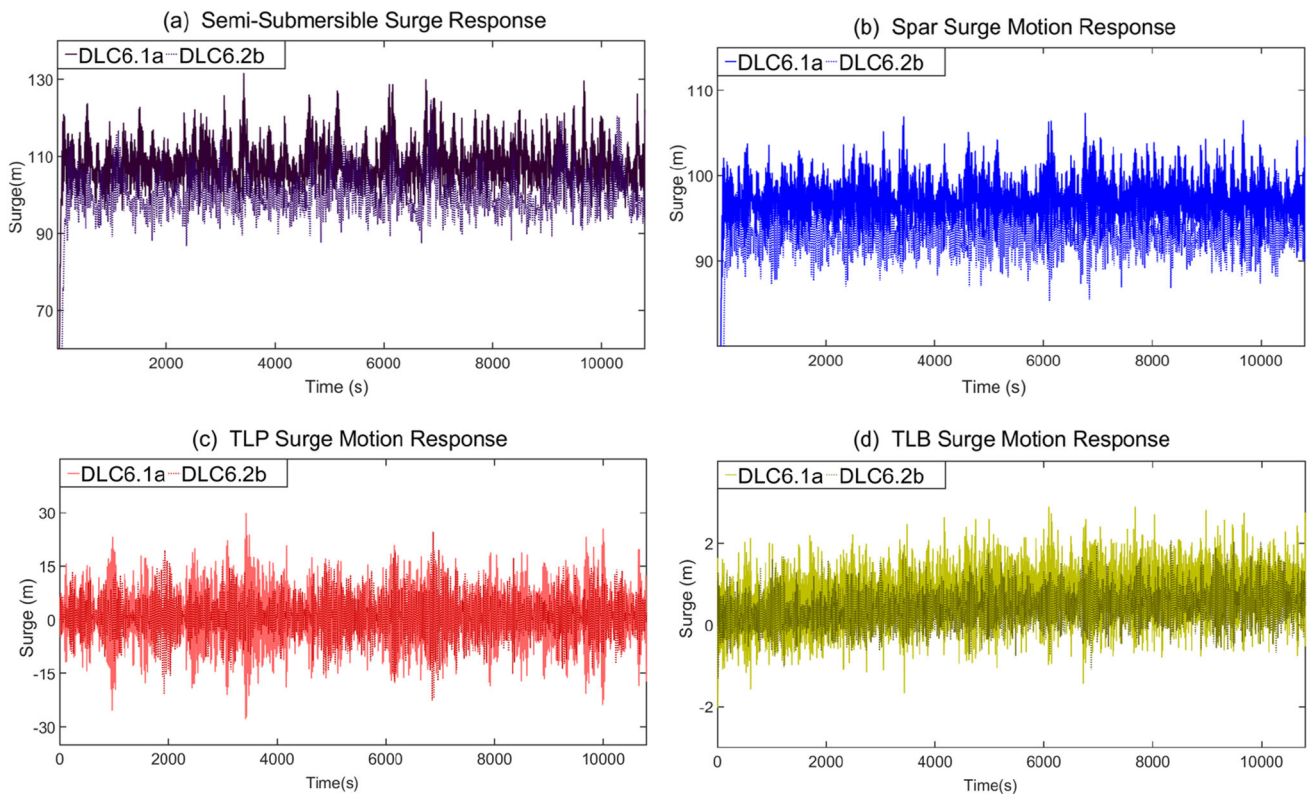
Fig. 32 DLC6.1a and DLC6.2b time history comparison of surge motion response for Semi-submersible (**a**), Spar (**b**), TLP (**c**), TLB (**d**)

Table 14 Maximum motion and most loaded maximum dynamic tension response of Semi-submersible, Spar, TLP, and TLB platforms under DLC6.1a (wind turbulence) and DLC6.2b (steady wind) events

Response	Wind profile	Semi-Submersible	Spar	TLP	TLB
Surge (m)	Turbulence	131.63	107.36	29.94	2.90
	Steady	124.65	102.93	24.63	2.50
Sway (m)	Turbulence	1.31	1.11	− 2.32	0.97
	Steady	1.04	0.99	− 1.86	0.64
Heave (m)	Turbulence	5.18	2.18	− 5.32	− 1.58
	Steady	4.37	1.90	− 5.00	− 1.51
Roll (°)	Turbulence	1.27	2.53	0.58	− 0.89
	Steady	1.03	1.92	0.53	− 0.79
Pitch (°)	Turbulence	3.34	4.95	0.70	1.81
	Steady	2.78	3.71	0.65	1.53
Yaw (°)	Turbulence	9.98	− 6.37	4.41	− 1.57
	Steady	8.30	− 5.16	3.89	− 1.36
Tension (ton)	Turbulence	1682.63	1597.54	2548.89	1448.90
	Steady	1477.15	1432.06	2286.92	1332.48

tension. The surge and yaw motion responses are coupled with the highest dynamic tension response for the TLB platform under both DLCs events. The slight delay between maximum dynamic tension and motion responses is due to the different time steps in Simo and Riflex for motion and line tension. The maximum motion responses of Semi-submersible are higher than the Spar responses apart from roll and pitch motion due to platform design characteristics.

Similarly, the TLP responses are higher than those for the TLB platform except for roll and pitch motion responses due to the mooring system and platform design characteristics. Table 14 illustrates the maximum responses of the platforms under both survival conditions. It is noted that all platforms experienced higher response magnitude due to the wind turbulence intensity.
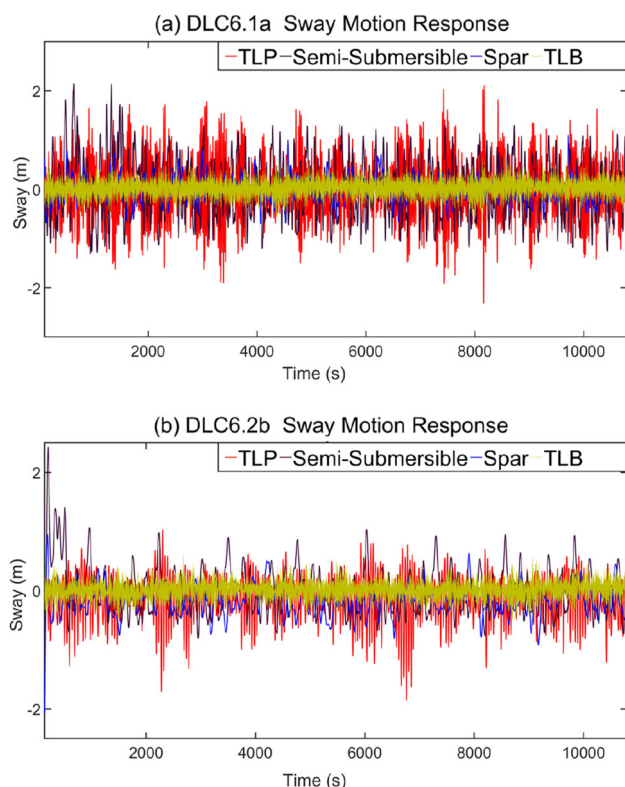
Fig. 33 Time history of sway motion responses for Semi-submersible, Spar, TLP, and TLB platforms under DLC6.1a (**a**) and DLC6.2b (**b**) events

Including wind turbulence led to increases in the motion response across all six degrees of freedom and the maximum recorded tension, the extent of increase compared to steady winds is shown in Fig. 31. This indicates a higher impact on the TLP surge response (22%) and the most negligible effect on the Spar surge motion responses (4%). The result of wind turbulence on the sway motion response of the TLP platform is 34% which is the highest among other platforms. In terms of heave motion response, the effect of turbulence on the TLP is the least (4%) and on the Semi-submersible is the highest (18%). The turbulence effect on the roll motion response of the Spar platform is 32% which is 8% more than that for the Semi-submersible platform, and it has a minor effect on the TLP platform by 8%. The induced effect of wind turbulence intensity on the pitch response of the Semi-submersible is 20% which is 13% less than that for the Spar. The impact of turbulence on TLP heave, roll, and pitch responses is less than that for the TLB due to the TLP design restraint in such motion directions. The minor effect of the wind turbulence intensity is shown on the TLB and TLP yaw responses (14% and 15%) whilst the highest is occurred for the Spar (23%). The wind turbulence has the highest impact on the Semi-submersible mooring lines. By comparing the dynamic tension of four platforms most loaded mooring line,

Semi-submersible mooring line has experienced maximum tension (14%).

The induced effect of the wind turbulence caused the surge and sway motion responses increased for the stiff systems more than the catenary, whilst wind turbulence has a more evident effect on the catenary systems in all other degrees of freedom.

Figure 32 shows the surge motion responses for all platforms under DLC6.1a and DLC6.2b events.

The TLB experienced an incredibly modest surge magnitude with high frequency among other platforms. The frequency of the Semi-submersible and Spar platform's surge oscillation is similar, but an excess peak is noted for the Semi-submersible platform. The effect of wind turbulence intensity on the mean surge motion response of the platforms with a catenary mooring system is more than that for platforms with a tension mooring system. The platforms with tension mooring lines had similar surge response behaviour, whether exposed to wind turbulence or steady; however, the peak magnitude is higher due to the wind turbulence intensity.

Figure 33a shows the impact of wind turbulence intensity on sway motion response, and Fig. 33b shows the time history of the surge motion response of four platforms under the steady wind. The sway response fluctuates, and peak response increases for all four platforms due to wind turbulence. The mean value remains similar, but peaks are clearly caused by wind turbulence. TLB shows a small sway response among other platforms with slight variation between turbulent and non-turbulence inflow, indicating that survival condition is less affected by the input wind. As the TLP platform is designed to be flexible in sway direction, it has the highest maximum sway response under DLC6.1a and is reduced to 1.9 m under the steady wind.

An apparent impact of wind turbulence on all platform heave motion responses can be seen by comparing Fig. 34a and b. It can be noted that the wind turbulence impact on the Semi-submersible and Spar platform's heave motion responses is higher than for TLP and TLB platforms. However, the TLP platform is designed to be restricted in the heave direction; a significant offset of the platform caused a setdown. Hence, the TLP has 5.3 m set down due to the platform offset. The TLP setdown caused the TLP maximum heave response to be more than the one for the TLB platform. Similarly, due to platform structure configuration and complexity, the Semi-submersible has more maximum heave response than the Spar platform under DLC6.1a and DLC6.2b.

Time history roll response for all platforms under DLC6.1a and 6.2b shown in Fig. 35, indicate that the roll amplitude for the Spar platform continued to increase at a rate higher than those for the Semi-submersible platform. The Semi-submersible roll motion response fluctuated more
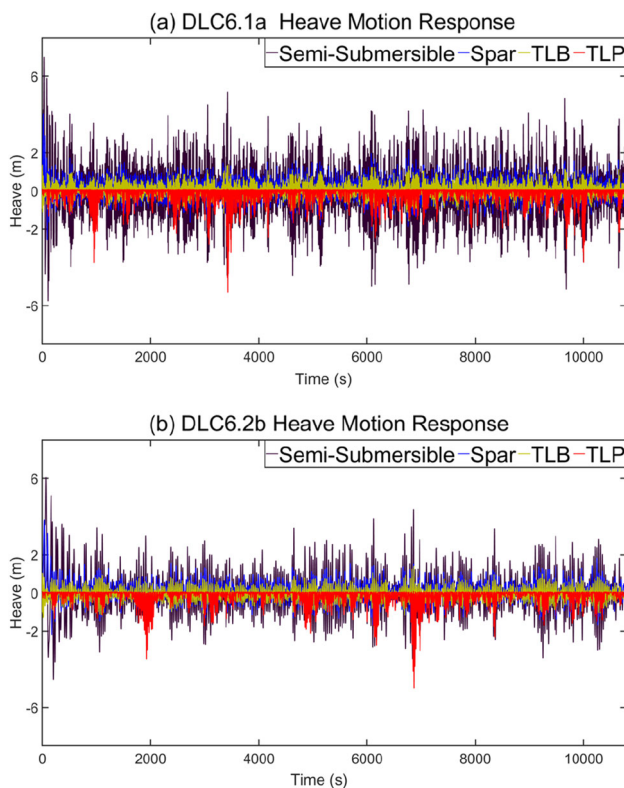
Fig. 34 Time history of heave motion response for Semi-submersible, Spar, TLP, and TLB platforms under DLC6.1a (**a**) and DLC6.2b (**b**) events
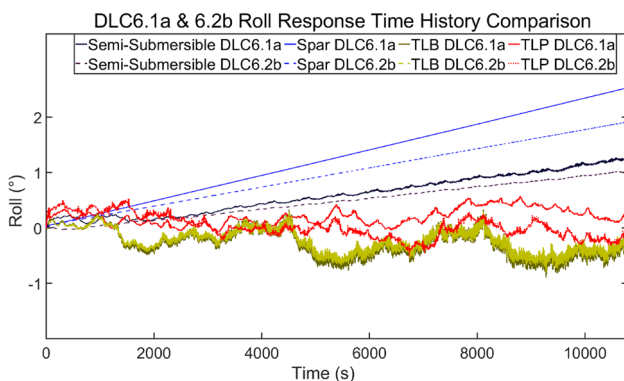

Fig. 35 Time history of roll motion responses for Semi-submersible, Spar, TLP, and TLB platforms under DLC6.1a and DLC6.2b events

while wind turbulence operated than when applied steady wind. Due to platform and mooring system designs and configurations, the TLP and TLB have fluctuated rolling under both survival conditions. The peak roll magnitude achieved for the Spar platform under DLC6.1a is more than the same case for the Semi-submersible platform due to multiple columns and pontoons for Semi-submersible to achieve stability compared with a buoyant cylinder with a deep draft. The TLB peak roll response is less than the TLP maximum

roll response because the TLP platform is designed to be eliminated the roll motion. For the same reason, the impact of wind turbulence on the TLP roll response is minor. The design configuration complexity exposed against a travelling wave direction played an essential role in roll motion response.

The time history of pitch motion response for the platforms under both design load cases in the survival condition case is shown in Fig. 36. The last 400 s is shown in bottom of Fig. 36. The pitch amplitude for the Spar platform continued to increase at a rate higher than those of other platforms. However, the TLP and TLB platforms experienced a high pitch response gradient at the early stage of the simulation, reaching their equilibrium and stabilising pitch direction during the simulation period. The Spar platform experienced more effect from the wind turbulence, and the TLP had less and changed minimally. The platforms with tension mooring systems experienced more frequency oscillation and less magnitude pitch response. Whilst the results showed that the platforms with catenary mooring systems have high pitch magnitude and less fluctuation, indicating that the mooring system and platform design characteristics played an essential role in pitch response.

The time history comparison of the yaw responses of the platforms under survival conditions with and without wind turbulence is shown in Fig. 37, where the impact of turbulence on yaw motion tends to lead to the Semi-submersible oscillating more than that for other platforms. The Semi-submersible platform achieved the highest maximum yaw motion under survival conditions, whilst TLB experienced a minor yaw response. A possible explanation is an assumption made to have a 20° spread of the fairlead attachment to replicate the effects of a bridle/delta connection to reduce the yaw motion of the TLB platform, which may not be the most suitable arrangement for the Semi-submersible and Spar Platforms. Hence, the methodology applied to the stiffness to model a bridle/delta connection may have to be revised for the Semi-submersible and Spar platforms to minimise the yaw motion response. The catenary mooring platforms oscillate in the yaw direction with higher amplitude than the tension mooring system platforms. The wind turbulence has impacted the magnitude of the platform's yaw response while not influencing the mean line yaw response. The impact of wind turbulence on the TLP platform yaw response behaviour is more evident than that for other platforms.

Figure 38 shows the most loaded line dynamic tension for the Semi-submersible (a), Spar (b), TLP (c), and TLB (d) platforms. shows the most loaded line dynamic tension for the Semi-submersible (a), Spar (b), TLP (c), and TLB (d) platforms. The Semi-submersible obtained more oscillation with a higher magnitude of dynamic tension response than the Spar platform because the Semi-submersible dynamic tension is coupled with surge and heave, and yaw responses
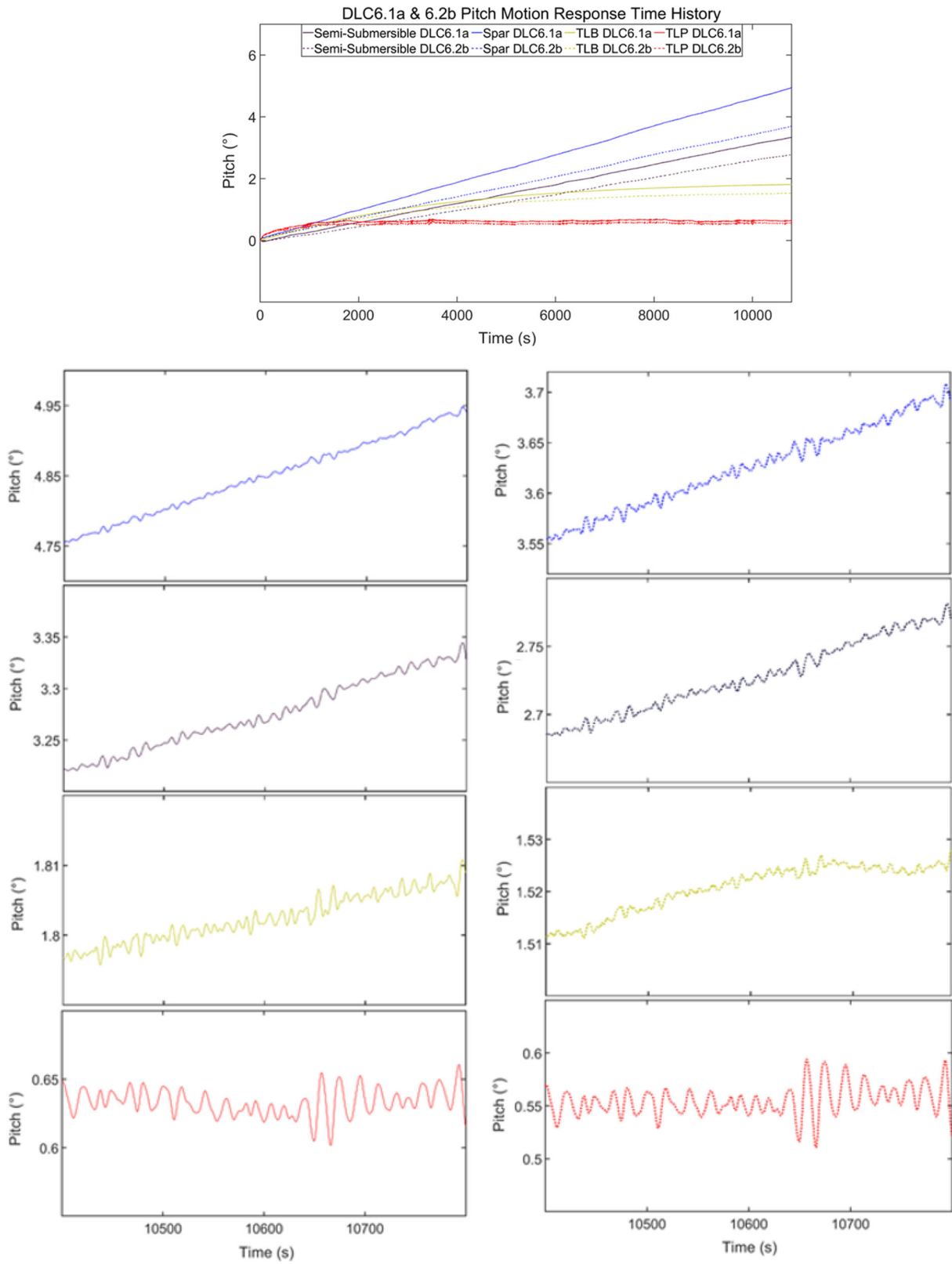
Fig. 36 Full time history (top) and last 400 s (bottom) of pitch motion responses for Semi-submersible, Spar, TLP, and TLB Platforms under DLC6.1a and DLC6.2b events
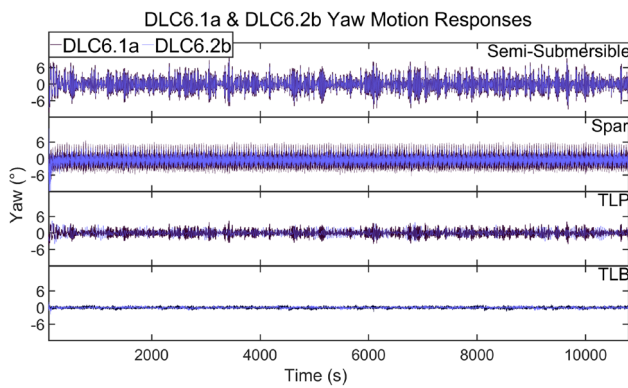
Fig. 37 Time history of yaw motion responses for Semi-submersible, Spar, TLP, and TLB platforms under DLC6.1a and DLC6.2b events

whilst the surge and tension for the Spar platform are coupled. However, the mean line tension for the Semi-submersible platform is less than that for the Spar due to the smaller mooring length. It is noted that wind turbulence has less effect on TLB mean tension response than other platforms. The higher impact of wind turbulence on the TLP platform than the TLB is due to the TLP design characteristics and its mooring system design. In addition, the TLB dynamic tension is coupled with surge and yaw motion responses. The TLP platform experienced maximum yaw response, then faced maximum

surge and heave responses concurrently followed by highest pitching, which consequences maximum dynamic tension.

The most loaded line's dynamic tension will evaluate according to DNV-OS-J103 (Veritas 2013) rules and regulations. The characteristic capacity of the mooring lines, S_C, is given in DNV-OS-J103 (Veritas 2013) calculates as $S_C = 0.95 S_{mbs}$ where S_{mbs} is the minimum breaking strength (MBL). The design criterion for ULS is given in DNV-OS-J103 express by $S_C > T_d$ where T_d is the design tension and calculate as $T_d = \gamma_{mean}.T_{c, mean} + \gamma_{dyn}.T_{c, dyn}.\gamma_{mean}$ and γ_{dyn} are load factors given in Table 15, $T_{c, mean}$ is the characteristic mean tension, and $T_{c, dyn}$ is the characteristic dynamic tension.

The design criteria for ULS given in DNV-OS-J103 (Veritas 2013) is that the characteristic capacity of the mooring line should be greater than the mooring line design tension. The design tension and characteristic capacity of each platform mooring line were calculated using considering the normal safety class load factor illustrated in Table 16.

The safety factor calculated shown in Table 17 indicates that all platform mooring lines comply with DNV regulation for mooring of FOWTs criteria. However, the design tension of the Semi-submersible mooring line is close to its characteristic capacity due to experiencing higher motion responses. The impact of wind turbulence intensity on the mooring line dynamic tension is evident. Due to the high MBL of the TLP
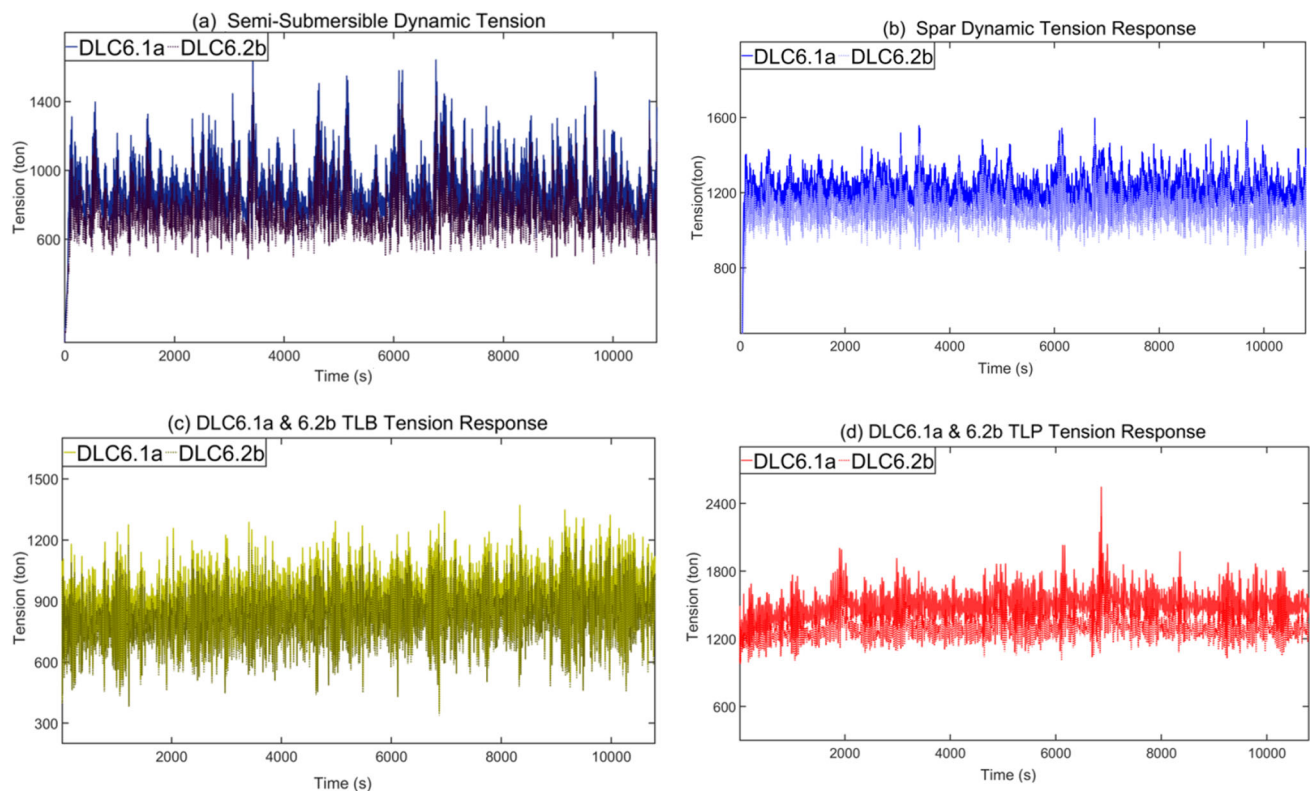

Fig. 38 DLC6.1a and DLC6.2b time history comparison of dynamic tension response for Semi-submersible (**a**), Spar (**b**), TLP (**c**), TLB (**d**)

Table 15 Mooring lines design load factor requirements

Limit state	Load factor	Safety class	
		Normal	High
ULS	γ_{mean}	1.30	1.50
ULS	γ_{dyn}	1.75	2.2

Table 16 Characteristic capacity and the design tension calculations of the mooring lines under survival conditions

		$T_d(N)$	
Platform	$S_C(N)$	DLC6.1a	DLC6.2b
Semi-Submersible	2.60E+07	2.50E+07	2.20E+07
Spar	2.60E+07	2.21E+07	1.99E+07
TLP	6.06E+07	3.71E+07	3.35E+07
TLB	2.80E+07	2.09E+07	1.92E+07

Table 17 The most loaded mooring line safety factors under survival conditions

Platform	DLC6.1a	DLC6.2b
Semi-submersible	1.04	1.18
Spar	1.17	1.31
TLP	1.63	1.81
TLB	1.34	1.46

mooring line, the safety factor calculated for the TLP platform is the highest among other platforms under both survival conditions.

6 Conclusion

This study has investigated four types of floating wind turbine support structures under operational and survival environmental conditions, including wind field descriptions covering simple steady, uniform wind to fluctuating turbulent wind. However, all four support platforms operate and maintain good motion in relatively severe sea states and satisfy the DNVGL-RP-0286 (DNV 2019) criteria. The TLB system has substantial advantages over the conventional floater and mooring types. First, as the TLB motion responses are reduced compared to other systems, specifically surge and pitch responses, the TLB design will allow for ease of adoption of land-based wind turbines without the need to re-develop control systems. Second, the TLB design is less prone to effects in wind turbulence, at least for the non-operating conditions evaluated in this paper. Third, the TLB

design is less complex than the current leading technology types for floating offshore wind platforms, simplifying the construction process. The TLB design could be ready built in the port, ballasted and then towed out to the deployed location, and by de-ballasting, the TLB can hook into the mooring lines. As a result, the expenditure on support vessels will be reduced. Therefore, the TLB design will provide a cost-effective, flexible alternative platform solution for large-scale FOWT development around the UK. Fourth, the design comparison has shown long section of lines on the seabed in the catenary mooring system. The innovative taut mooring system designed for the TLB system is advantageous over the catenary mooring line. The taut mooring system does not touch the seabed. Another advantage of the taut mooring system is that it can deploy more platforms in the limited wind farm area due to the surge motion response being considerably less than the platforms with catenary mooring and TLP-type platforms. The maximum tension recorded for the TLB maximum loaded line under survival conditions is the lowest for other platforms and below the MBF of the respective line materials. The increased costs of additional lines could be offset by savings in installation and the potential for connecting multiple turbines mooring lines to a single anchor, therefore achieving potential reaction force reactions, and reducing the number of anchors installed.

Finally, this study showed that the TLB platform will be able to produce more power than other considered platforms.

Further study should be conducted to investigate the system performance under non-collinear environmental conditions and include turbulent wind modelling during offshore wind turbine operation. A detailed cost analysis study should also be performed to allow a clear perspective of the most cost-effective design.

Declarations

References

ACTEON (2021) Intermoor-world leader in mooring technology. https://acteon.com/moorings-anchors/intermoor/. Accessed 2021

Adam F, Myland T, Dahlhaus F, Großmann J (2014) Scale tests of the GICON®-TLP for wind turbines. In: ASME 2014 33rd international conference on ocean, offshore and arctic engineering, American Society of Mechanical Engineers Digital Collection

Alexandre A, Percher Y, Choisnet T, Buils Urbano R, Harries R (2018) Coupled analysis and numerical model verification for the 2MW Floatgen demonstrator project with IDEOL platform. In: ASME 2018 1st international offshore wind technical conference, San Francisco, California, USA. American Society of Mechanical Engineers Digital Collection

Al-Solihat MK, Nahon M (2016) Stiffness of slack and taut moorings. Ships Offshore Struct 11(8):890–904

Amano RS (2017) Review of wind turbine research in 21st century. J Energy Resour Technol. https://doi.org/10.1115/1.4037757

Bak C, Zahle F, Bitsche R, Kim T, Yde A, Henriksen LC, Hansen MH, Blasques FPAA, Gaunaa M, Natarajan A (2013) The DTU 10-MW reference wind turbine. Danish Wind Power Research 2013. Trinity, Denmark, 27–28 May 2013

Borg M, Collu M (2015) A comparison between the dynamics of horizontal and vertical axis offshore floating wind turbines. Philos Trans R Soc A Math Phys Eng Sci 373(2035):20140076

Bossler A (2013) Japan's floating offshore wind projects: an overview. Maine Ocean and Wind Industry Initiative: MOWII Webinar (May 2013)

BRIDON BEKAERT (2020) Market leading rope solutions for offshore oil & gas. https://www.bridon-bekaert.com/en-gb. Accessed 2020

Bulder B, van Hees M, Henderson A, Huijsmans R, Pierik J, Snijders E, Wijnants G, Wolf M (2002) Study to feasibility of and boundary conditions for floating offshore wind turbines. ECN MARIN TNO TUD MSC Lagerway Windmaster 26:70–81

Butterfield S, Musial W, Jonkman J, Sclavounos P (2007) Engineering challenges for floating offshore wind turbines. National Renewable Energy Laboratory (NREL), Golden

Carbon Trust (2015) Floating offshore wind: market and technology review. Report prepared for the Scottish Government, June 2015

Castro-Santos L, Diaz-Casas V (2016) Floating offshore wind farms. Springer, Cham

CATAPULT (2018) Macroeconomic benefits of floating offshore wind in the UK. Industry Report, 29 October 2018

CATAPULT (2018) Macroeconomic benefits of floating offshore wind in the UK. 5bd78f98e76ae_Macroeconomic benefits of offshore wind in the UK -October 2018 (2).pdf. Accessed 04 Feb 2019

Cermelli C, Roddier D, Weinstein A (2012) Implementation of a 2MW floating wind turbine prototype offshore Portugal. In: Offshore technology conference

Coulling AJ, Goupee AJ, Robertson AN, Jonkman JM (2013) Importance of second-order difference-frequency wave-diffraction forces in the validation of a FAST semi-submersible floating wind turbine model. (55423):V008T009A019

Crozier A (2011) Design and dynamic modeling of the support structure for a 10 MW offshore wind turbine. Institutt for energi-og prosessteknikk, Trondheim

DNV G (2019) Recommended practice: coupled analysis of floating wind turbines. DNVGL-RP-0286. DNV GL AS, Høvik, Oslo, Norway

Equinor (2018) Hywind—leading floating offshore wind solution. https://www.equinor.com/en/what-we-do/hywind-where-the-wind-takes-us.html. Accessed 6 Nov 2018

Faltinsen O (1993) Sea loads on ships and offshore structures. Cambridge University Press, Cambridge

Fukushima Offshore (2014) Fukushima floating offshore wind farm demonstration project (Fukushima FORWARD). https://www.offshorewind.biz/2014/10/30/fukushima-offshore-floating-wind-project-moves-forward/

Fulton G, Malcolm D, Moroz E (2006) Design of a semi-submersible platform for a 5MW wind turbine. In: 44th AIAA aerospace sciences meeting and exhibit, 09–12 January 2006. Reno, Nevada, USA

George J (2014) WindFloat design for different turbine sizes. Master's thesis project, Instituto Superior Técnico Technical University of Lisbon, Portugal, MS

Henderson A, Leutz R, Fujii T (2002) Potential for floating offshore wind energy in Japanese waters. In: Proceedings of the twelfth (2002) international offshore and polar engineering conference, 26–31 May 2002, Kitakyushu, Japan

Henderson AR, Witcher D (2010) Floating offshore wind energy—a review of the current status and an assessment of the prospects. Wind Eng 34(1):1–16

International renewable Energy Agency (IRENA) (2016) Floating foundations: a game changer for offshore wind power. https://www.irena.org/-/media/Files/IRENA/Agency/Publication/2016/IRENA_Offshore_Wind_Floating_Foundations_2016.pdf. Accessed 12 Mar 2019

James R, Ros MC (2015) Floating offshore wind: market and technology review. The Carbon Trust, London

James R, Weng W-Y, Spradbery C, Jones J, Matha D, Mitzlaff A, Ahilan R, Frampton M, Lopes M (2018) Floating wind joint industry project—phase I summary report. Carbon Trust Tech Rep 19:2–20

Jonkman BJ (2009) TurbSim user's guide: version 150. National Renewable Energy Lab (NREL), Golden

Jonkman J (2010a) Definition of the floating system for phase IV of OC3. National Renewable Energy Laboratory (NREL), Golden

Jonkman J (2010b) Index of/public/jjonkman/NRELOffshrBsline5MW. http://wind.nrel.gov/public/jjonkman/NRELOffshrBsline5MW/

Jonkman J, Sclavounos P (2006) Development of fully coupled aeroelastic and hydrodynamic models for offshore wind turbines. In: 44th AIAA aerospace sciences meeting and exhibit, 09–12 January 2006. Reno, Nevada, USA

Jonkman JM, Buhl ML Jr (2007a) Loads analysis of a floating offshore wind turbine using fully coupled simulation. National Renewable Energy Lab. (NREL), Golden

Jonkman JM, Buhl ML Jr (2007b) Loads analysis of a floating offshore wind turbine using fully coupled simulation. In: Wind power conference and exhibition, Los Angeles, CA

Kolios A, Rodriguez-Tsouroukdissian A, Salonitis K (2016) Multicriteria decision analysis of offshore wind turbines support structures under stochastic inputs. Ships Offshore Struct 11(1):38–49

Lee KH (2005) Responses of floating wind turbines to wind and wave excitation. Massachusetts Institute of Technology, Cambridge

Lee C-H, Newman J (2005) Computation of wave effects using the panel method. In: WIT transactions on state-of-the-art in science and engineering 18.

Leimeister M, Kolios A, Collu M (2018) Critical review of floating support structures for offshore wind farm deployment. J Phys Conf Ser 1104:012007

Liu Y, Li S, Yi Q, Chen D (2016) Developments in semi-submersible floating foundations supporting wind turbines: a comprehensive review. Renew Sustain Energy Rev 60:433–449

Liu Y, Xiao Q, Incecik A, Peyrard C, Wan D (2017) Establishing a fully coupled CFD analysis tool for floating offshore wind turbines. Renew Energy 112:280–301

Maciel JG (2010) The WindFloat project. Lisbon: edp: 24

Madsen PH, Risø D (2008) Introduction to the IEC 61400–1 standard. Risø National Laboratory, Technical University of Denmark, Roskilde

Mahfouz MY, Molins C, Trubat P, Hernández S, Vigara F, Pegalajar-Jurado A, Bredmose H, Salari M (2021) Response of the International Energy Agency (IEA) Wind 15 MW WindCrete and Activefloat floating wind turbines to wind and second-order waves. Wind Energy Sci 6(3):867–883

Mast E, Rawlinson R, Sixtensson C (2015) Market study floating wind in the Netherlands: potential of floating offshore wind. TKI Wind op Zee, DNV GL

Matha D (2010) Model development and loads analysis of an offshore wind turbine on a tension leg platform with a comparison to other floating turbine concepts: April 2009. National Renewable Energy Lab. (NREL), Golden

Matha D, Sandner F, Molins C, Campos A, Cheng PW (2015) Efficient preliminary floating offshore wind turbine design and testing methodologies and application to a concrete spar design. Philos Trans R Soc A 373(2035):20140350

Musial W, Butterfield S, Ram B (2006) Energy from offshore wind: preprint. National Renewable Energy Laboratory (NREL), Golden

Myhr (2016) Developing offshore floating wind turbines: the Tension-Leg-Buoy design. PhD Thesis, Norwegian University of Life Science

Myhr A, Maus KJ, Nygaard TA (2011) Experimental and computational comparisons of the OC3-HYWIND and tension-leg-buoy (TLB) Floating Wind Turbine Conceptual Designs. In: The twenty-first international offshore and polar engineering conference, Maui, Hawaii, USA, International Society of Offshore and Polar Engineers, p 8

Myhr A, Bjerkseter C, Ågotnes A, Nygaard TA (2014) Levelised cost of energy for offshore floating wind turbines in a life cycle perspective. Renew Energy 66:714–728

Nilsson D, Westin A (2014) Floating wind power in Norway analysis of future opportunities and challenges. MS thesis, Lund University, Sweden

Paulsen US, Vita L, Madsen HA, Hattel J, Ritchie E, Leban KM, Berthelsen PA, Carstensen S (2012) 1st DeepWind 5 MW baseline design. Energy Procedia 24:27–35

PFOWF (2022) Environmental statement: offshore non-technical summary. https://marine.gov.scot/sites/default/files/eia_report_volume_1_-_non-technical_summary_redacted.pdf. Accessed 23 Nov 2022

PrinciplePower (2022) Kincardine Offshore Windfarm. https://www.principlepower.com/projects/kincardine-offshore-wind-farm. Accessed 2022

Ramzanpoor I, Nuernberg M, Tao L (2019) Coupled numerical analysis of a concept TLB type floating offshore wind turbine. In: ASME 2019 38th international conference on ocean, offshore and arctic engineering, Glasgow, UK. American Society of Mechanical Engineers Digital Collection

Roald L, Jonkman J, Robertson A, Chokani N (2013) The effect of second-order hydrodynamics on floating offshore wind turbines. Energy Procedia 35:253–264

Robertson A, Jonkman J, Masciola M, Song H, Goupee A, Coulling A, Luan C (2014) Definition of the semisubmersible floating system for phase II of OC4. National Renewable Energy Lab. (NREL), Golden

Robertson AN, Jonkman JM (2011) Loads analysis of several offshore floating wind turbine concepts. In: The twenty-first international offshore and polar engineering conference, International Society of Offshore and Polar Engineers, Maui, Hawaii, USA

Rodrigues S, Restrepo C, Kontos E, Pinto RT, Bauer P (2015) Trends of offshore wind projects. Renew Sustain Energy Rev 49:1114–1135

Sclavounos P, Lee S, DiPietro J, Potenza G, Caramuscio P, De Michele G (2010) Floating offshore wind turbines: tension leg platform and taught leg buoy concepts supporting 3-5 MW wind turbines. In: European wind energy conference EWEC, pp 20–23. Warsaw, Poland, 20–23 April 2010

Singhal G, Connolly A, Laranjinha M, McKinnon C, Mortimer A (2021). Independent assessment of current floater concepts for floating wind application. In: SNAME 26th offshore symposium, 06–07 April 2021 (Virtual). OnePetro

Statoil (2017) Statoil to build the world's first floating wind farm: Hywind Scotland. https://www.statoil.com/en/news/hywindscotland.html. Accessed 15 Jan 2018

Sugianto DN, Zainuri M, Darari A, Suripin S, Darsono S, Yuwono N (2017) Wave height forecasting using measurement wind speed distribution equation in Java Sea, Indonesia. Int J Civ Eng Technol 8(5):604–619

Taboada JV (2015) Comparative analysis review on floating offshore wind foundations (FOWF). In: Proceedings of the 54th naval engineering and maritime industry congress, Ferrol, Spain

Tracy CCH (2007) Parametric design of floating wind turbines. Massachusetts Institute of Technology, Cambridge

Trolle J, Hornbak F (2016) Optimization of tension leg buoy with regards to stabilization failure. Master's thesis, Aalborg University Esbjerg, Esbjerg, Denmark

Veritas DN (1994) Wave analysis by diffraction and Morison theory (WADAM). SESAM user's manual. Det Norske Veritas (DNV), Høvik

Veritas DN (2004) DNV-OS-J101-design of offshore wind turbine structures. Det Norske Veritas, Høvik

Veritas DN (2010) Recommended practice DNV-RP-C205: environmental conditions and environmental loads. DNV, Høvik

Veritas DN (2013) DNV-OS-J103: design of floating wind turbine structures. DNV, Høvik

Vindenes H, Orvik KA, Søiland H, Wehde H (2018) Analysis of tidal currents in the North Sea from shipboard acoustic Doppler current profiler data. Cont Shelf Res 162:1–12

Vita L, Ramachandran G, Krieger A, Kvittem MI, Merino D, Cross-Whiter J, Ackers BB (2015) Comparison of numerical models and verification against experimental data, using Pelastar TLP concept. In: ASME 2015 34th international conference on ocean, offshore and arctic engineering, American Society of Mechanical Engineers

Wayman EN, Sclavounos P, Butterfield S, Jonkman J, Musial W (2006) Coupled dynamic modeling of floating wind turbine systems: preprint. National Renewable Energy Lab. (NREL), Golden

Withee JE (2004) Fully coupled dynamic analysis of a floating wind turbine system. Naval Postgraduate School, Monterey

Witte T, Siegfriedsen S, El-Allawy M (2003) WindDeSalter® technology direct use of wind energy for seawater desalination by vapour compression or reverse osmosis. Desalination 156(1–3):275–279

Zhao J, Zhang L, Wu H (2012) Motion performance and mooring system of a floating offshore wind turbine. J Mar Sci Appl 11(3):328–334

Zwick D, Muskulus M (2016) Simplified fatigue load assessment in offshore wind turbine structural analysis. Wind Energy 19(2):265–278